Effect of Sn Doping of Sol-gel Processed ZnO Electron Transport Layer on the Photovoltaic Performance in P3HT:PCBM-based Organic Solar Cell

Biruk Alebachew Seid

A Thesis Submitted to

The Department of Materials Science and Engineering

School of Mechanical, Chemical, and Materials Engineering

Presented in Partial Fulfillment of the Requirement for the Degree of Master's in Materials Science and Engineering

Office of Graduate Studies

Adama Science and Technology University

June, 2022

Adama, Ethiopia

Effect of Sn Doping of Sol-gel Processed ZnO Electron Transport Layer on the Photovoltaic Performance in P3HT:PCBM-based Organic Solar Cell

Mr. Biruk Alebachew Seid

Advisor: Dr. Temesgen Debelo Dessisa

Co- Advisor: Dr. Newayemedhin Tegegne Aberra

A Thesis Submitted to

The Department of Materials Science and Engineering

School of Mechanical, Chemical, and Materials Engineering,

Presented in Partial Fulfillment of the Requirement for the Degree of Master's in material science and engineering

Office of Graduate Studies

Adama Science and Technology University

June, 2022

Adama, Ethiopia

DECLARATION

I hereby declare that this Master Thesis entitled **"Effect of Sn doping of sol-gel processed ZnO electron transport layer on the photovoltaic performance in P3HT:PCBM-based organic solar cell"** is my original work. That is, it has not been submitted for the award of any academic degree, diploma, or certificate in any other university. All sources of materials that are used for this thesis have been duly acknowledged through citation.

_____	_____	_____
Name of the Student	Signature	Date

RECOMMENDATION

I/we, the advisor(s) of this thesis, hereby certify that I/we have read the revised version of the thesis entitled "**Effect of Sn doping of sol-gel processed ZnO electron transport layer on the photovoltaic performance in P3HT:PCBM-based organic solar cell**" prepared under my/our guidance by Biruk Alebachew Seid submitted in partial fulfillment of the requirements for the degree of Master's of Science in **Materials Science and Engineering**

Therefore, I/we recommend the submission of revised version of the thesis to the

Department following the applicable procedures.

_____ _____ _____

Major Advisor Signature Date

_____ _____ _____

Co-advisor Signature Date

APPROVAL SHEET

I/we, the advisors of the thesis entitled **"Effect of Sn doping of sol-gel processed ZnO electron transport layer on the photovoltaic performance in P3HT:PCBM-based organic solar cell"** and developed by Biruk Alebachew Seid hereby certify that the recommendation and suggestions made by the board of examiners are appropriately incorporated into the final version of the thesis.

Major Advisor	Signature	Date

We, the undersigned, members of the Board of Examiners of the thesis by Biruk Alebachew Seid have read and evaluated the thesis entitled **"Effect of Sn doping of sol-gel processed ZnO electron transport layer on the photovoltaic performance in P3HT:PCBM-based organic solar cell"** and examined the candidate during the open defense. This is, therefore, to certify that the thesis is accepted for partial fulfillment of the requirement of the degree of Master of Science in Material science and engineering.

Chairperson	Signature	Date
Internal Examiner	Signature	Date
External Examiner	Signature	Date

Finally, approval and acceptance of the thesis are contingent upon the submission of its final copy to the Office of Postgraduate Studies (OPGS) through the Department Graduate Council (DGC) and School Graduate Committee (SGC).

Department Head	Signature	Date
School Dean	Signature	Date
Office of Postgraduate Studies,	Dean Signature	Date

ACKNOWLEDGMENT

Fabrication of solar cell devices and characterization were carried out at materials physics and polymer lab at Addis Ababa University, I strongly acknowledge Addis Ababa University. I would like to further acknowledge Adama Science and Technology University (ASTU) for giving me the MSc opportunity and research fund to accomplish this research. I am greatly indebted to my co-advisor, Dr. Newayemedhin Tegegne, for her multifaceted support, notably academic guidance, material and financial support, love and patience, without which this achievement would not have been reached. The presentations I had in several times with your research group helped me understand the materials and interpret the measurements in solar cells. My heartfelt thanks must also to my advisor Dr. Temesgen Debelo for supervising and motivating me to work on photovoltaic. Thank you for being my advisor and providing me with the basic knowledge in research from my undergraduate degree final project to postgraduate degrees of this thesis work. My thanks also extend to Mr. Demeke Tesfaye, and all staff members of the Materials Science and Engineering department. I would like to express my special thanks to my family. Your help throughout my life was immeasurable that putting smile on my face even in times I was frustrating. I am blessed to have family like you. I am also greatly indebted to the different researchers, and authors whose work I have quoted or referred to in my work. Finally we are grateful to all person contributed for successful completion of this work.

Table of Contents

LIST OF TABLES

LIST OF FIGURES

LIST OF ABBREVIATIONS

P3HT	poly (3 hexylthiophenes)
PCBM	[6,6]-phenyl-C61-butyric acid methyl ester
PCE	power conversion efficiency
FF	fill factor
J_{sc}	Short- circuit current density
V_{oc}	open-circuit voltage
J-V	current density-voltage
J_L	current density under illumination
J_D	current density in the dark
MPP	maximum power point
ETL	electron transport layer
CBL	cathode buffer layer
ABL	anode buffer layer
HTL	hole transport layer
ITO	Indium Tin Oxide
FTO	Fluorine Tin Oxide
TCO	transparent conductive oxide
OSCs	organic solar cells
ISC	Inverted solar cell
OPV	organic photovoltaic
OLEDs	Organic Light Emitting Diodes

BHJ	bulk heterojunctions
WF	work function
PEI	polyethylenimine
XRD	X-ray powder diffraction
UV-vis	Ultraviolet-Visible spectroscopy
PL	Photoluminescence spectroscopy,
SEM	Scanning Electro-Microscope
EDS	Energy Dispersion Spectroscopy
RS	Raman Spectroscopy
AFM	atomic force microscopy
LUMO	lowest unoccupied molecular orbital
HOMO	highest occupied molecular orbital
LD	Diffusion length
CZO	Cd-doped ZnO
AZO	Al-doped ZnO
ZTO	Sn-doped ZnO
EDT	Ethanedithiol
CF	Chloroform
LO	longitudinal optical
TO	transverse optical
DARS	disorder-activated Raman scattering
QE	quenching efficiency
SCLC	space limited current

ABSTRACT

Zinc Oxide (ZnO) films made at low temperature by sol-gel process are one of the best electron-transporting layers (ETLs) for high-performance organic solar cells (OSCs) due to the absence of pinholes, ease of preparation, thickness controllability, and processability at low temperature. The charge mobility and electrical conductivity of ZnO films prepared at low temperatures, on the other hand, are lower, resulting in a decrease in photovoltaic performance. In this work, pristine and Sn-doped ZnO thin films were prepared via the sol-gel method at a low temperature as electron transporting layers (ETLs) in poly (3 hexylthiophenes) and [6,6]-phenyl-C61-butyric acid methyl ester (P3HT:PCBM) blend OSCs device. To investigate the effect of Sn dopant on the properties of ZnO thin films, the dopant concentrations varied from 1 %, 2 %, 3 %, and 5 % weight percentages. The highest power conversion efficiency (PCE) of about 3.45 % was measured on the sample with a 3 wt. % of Sn dopant, which is an increase of almost 340 % compared to the PCE of the ZnO-only device (1.01 %). It was found that Sn-doped ETL exhibited an improvement in electrical conductivity by more than two folds and reduced electron trapping defect states which is beneficial for enhanced transport of the dissociated electron from the active layer. Moreover, the device with Sn-doped ZnO exhibited an enormous improvement in exciton generation and dissociation efficiency in addition to enhanced charge mobility, especially for the device at an optimum dopant concentration of 3 wt.%. The combined effect of all these properties attributed to an increment of current density (J_{sc}), open-circuit voltage (V_{oc}), and fill factor (FF) by 200 %, 140 %, and 130 %, respectively, in the 3 wt% Sn doped device compared to the reference device, resulting in improved photovoltaic performance. These results imply that Sn-doped ETLs enable efficient metal oxide ETL in P3HT-based OSCs, and we believe that the active layer is not limited to polymers used in this work and can also be used in flexible solar cell applications because of annealing at low-temperatures.

Keywords: *Organic solar cells, Power conversion efficiency, Sn-doped Zinc Oxide, Electron Transport Layer, Charge mobility*

CHAPTER ONE

1. INTRODUCTION

1.1. Background of the study

Solar energy is the most promising and efficient source of energy among the numerous energy sources (Roy, Sinha, Tiwari, & Khare, 2020). Because the sun's annual solar radiation produces significantly more energy than the entire world's population consumes in a year, photovoltaic cells to harvest the sun's energy have received a lot of attention (Wöhrle & Meissner, 1991; You, Dou, et al., 2013).

Because of the recent introduction of active layer materials, interfacial layers, and device architecture, organic photovoltaics (OPVs) have progressed considerably in terms of their power conversion efficiencies (PCEs) (S.-H. Liao et al., 2014; Steim, Kogler, & Brabec, 2010). Organic solar cells (OSCs) have a photoactive layer made up of donor and acceptor materials arranged in a layer-by-layer pattern to produce bilayer heterojunctions or blended together to generate bulk heterojunctions (BHJ). For the formation of all the excitons within the diffusion length in an interconnected network of the donor and acceptor phases, donor and acceptor materials in the form of a blend are preferable compared to layer-by-layer geometry, whereas the latter has the disadvantage of a short diffusion length (Peumans, Yakimov, & Forrest, 2003; Wan, Long, Huang, & Chen, 2011). For example, a phase-separated (BHJ) nanostructure formed by a blend of regioregular poly(3-hexylthiophene) (P3HT) and the fullerene derivative [6,6]-phenyl-C61 butyric acid methyl ester (PCBM) offers a large interfacial area for efficient exciton dissociation and is also the most widely researched donor and acceptor materials (You, Chen, et al., 2013).

Due to their possible lightweight, flexibility, low cost, and easy fabrication processes via solution processing compared to their inorganic counterparts, OSCs in the form of thin film are the most promising light-harvesting device in producing and providing sufficient cheap renewable energy (Ike, Hamed, & Mola, 2022). However, most of these OSCs have low PCEs and are environmentally unstable in the presence of moisture and oxygen. As a result, many researchers have been working on the synthesis of new and stable conjugated polymer and small molecule donors and fullerene acceptors, as well as interface engineering, controlling the morphology of the

photoactive layer (W. Ma et al., 2014; Y. Sun et al., 2012), and designing and implementing of new device architectures (T. Yang et al., 2012; You, Dou, et al., 2013) which now has greatly contributed to the increase in PCEs. Most OSCs have recently improved their power conversion efficiencies (PCEs), i.e. research has shown that device power conversion efficiency has surpassed 18% for single-junction solar cells (Yuanbao Lin et al., 2020).

Conventional and inverted configurations can be used to make bulk heterojunction cells. Despite their high PCEs, conventional PSCs have some drawbacks, such as lack of long-term stability when exposed to air and an acidic PEDOT:PSS interfacial layer that directly contacts the ITO glass and can etch the ITO (Kawano et al., 2006; Y. Sun, Seo, Takacs, Seifter, & Heeger, 2011). This prevents the practical application of the conventional device solar cells. On the one hand, the instability is due to the use of a low-work-function metal (e.g., Al) as the cathode, which is susceptible to oxygen and moisture and quickly oxidizes (Braid, 2016). This has led to the development of inverted structure polymer solar cells, in which inverted devices use an electron transport layer, such as ZnO, to collect electrons, avoiding the stability issues associated with both the PEDOT:PSS/ITO interface and water and oxygen diffusion into the low work function anode, which is typically Al or Ca/Al in traditional devices(Braid, 2016).

Although the active layer material (e.g., conjugated polymers and fullerenes) and device structure have a significant impact on the PCE, the electron transfer buffer layers used as an interfacial layer between the photoactive layer and the cathode also play a key role(Wei, Yin, Chen, & Zheng, 2017). This is due to the establishment of ohmic contact, modification of the internal electric field, and reduction of carrier recombination rate (Yip & Jen, 2012) thereby allowing efficient exciton dissociation, charge collection, and charge extraction through chemical reactions, geometry modification, and/or inducing interfacial charge redistribution processes (Adedeji, Hamed, & Mola, 2020).

Zinc oxide (ZnO) has been employed widely as an ETL in inverted OSCs devices because of its high visible light transparency, air stability, strong electron affinity, solution processability, and tunable optical and electrical properties (Park, Lim, Kim, & Jang, 2013). Moreover, its conduction band edge is at around 4.2 eV, which is lower than that of the poly (3 hexylthiophenes) (P3HT) and [6,6]-phenyl- (PCBM) blend. Moreover, the election mobility of ZnO is relatively high at

around 200–300 $cm^2V^{-1}s^{-1}$ (Homnan et al., 2021), thus the ZnO has been proposed as an effective electron transporting layer (ETL) in OSCs applications.

Zinc oxide (ZnO) films made by the sol-gel process are one of the best electron-transporting layers (ETLs) for high-performance OSCs because of their low work function (WF) and ease of production (Wei et al., 2017). Although ZnO prepared in this way is a suitable material for an ETL, the use of ZnO nanoparticles (NPs) can cause electron trapping and a high series resistance due to defects with absorbed oxygen and inhomogeneous spatial distribution of nanoparticles, limiting the performance of ZnO-based devices (Guo et al., 2000; Sakohara, Ishida, & Anderson, 1998; Small et al., 2012). To address this issue, several techniques such as high-temperature annealing, metallic nanocomposites/nanoparticles, and doping have been used and this will go a long way toward improving the performance in OSC applications(Guo et al., 2000; Sakohara et al., 1998; Small et al., 2012).

Sn inclusion into ZnO crystals is currently one of the most promising ways for improving the electrical conductivity of ZnO thin films (Ajili, Castagné, & Turki, 2013; F. Bedia, Bedia, Aillerie, Maloufi, & Benyoucef, 2015; Ilican, Caglar, & Caglar, 2010), and consequently the performance of OSCs. Several groups have reported low-temperature processed ZnO thin films that incorporate Sn nanoparticles into the ZnO as an electron transport layer to increase the performance of solar cells.

Wei, J., *et al*. reported Sn-doped ZnO by a sol-gel method, and employed as an electron transport material for organic solar cells (OSCs), obtained PCE of about 9 % for the ZnO film doped with Sn whereas the pristine film processed at the same temperature exhibit low PCE of 8 % (Wei et al., 2017). Moreover, the Sn-doped ZnO film annealed at 120 ˚C had PCE of 9 % compared to the film annealed at 200 ˚C (9.32 %). Malison, P., *et al.* utilized Sn-doped ZnO thin film processed at 160 ˚C as ETLs in perovskite solar cells and obtained improved photovoltaic performances due to the decrease in series resistance and increasing shunt resistance (Malison et al., 2019). Recently, Homnan, S., *et al.* reported a low-temperature Sn-doped ZnO thin film and found that an annealing temperature of 140 ˚C was high enough for precursor-to-Sn-doped ZnO conversion. A better power conversion efficiency of about 11 % was achieved compared to the one device annealed at high temperature with a PCE of 10.31 % (Homnan et al., 2021). The improvement is attributed to the increase in electrical conductivity by the combined effect of Sn dopant and temperature according

to the report (Homnan et al., 2021). Venkataraj. S. *et al.* investigated the effects of Sn doping on ZnO films at concentrations ranging from 4–6% (Venkataraj et al., 2009). They observed an increase in electron concentration and a decrease in electrical resistivity owing to Sn dopant, with $SnZn_2O_4$ emerging as the main phase. The electron mobility was decreased when the Sn concentration was above 10 % (Venkataraj et al., 2009). Sun *et al.* used low annealing temperatures below 200 °C to fabricate ZnO films by a sol-gel method. They demonstrated a reduction in the annealing temperature to 130 °C, leading to a decrease in PCE of OSC from 6% (at 200 °C) to 5.4 % (at 130 °C) as a result of a reduction in the electron mobility of ZnO film (Venkataraj et al., 2009). Chen, H.-C., *et al.* blended a low-temperature sol-gel processed ZnO solution with a polyethyleneimine (PEI) solution to form ZnO:PEI composite layer as the ETL layer and they recorded PCE of 8.7% compared to the pristine device(7.3 %) (H.-C. Chen, Lin, Jiang, Su, & Wei, 2015). The improvement is caused by the improved surface roughness of the ZnO films in the blend which resulted in the increment of the electron mobility in the vertical direction.

In this work, the inverted polymer solar cell based on P3HT:PCBM as active layer and room temperature sol-gel processed Sn-doped ZnO as ETLs with various concentrations of Sn (0,1,2,3, and 5 wt.%) were fabricated. To our best of knowledge, there is no reported work using Sn-doped ZnO as ETL for P3HT:PCBM solar cells. The incorporation of Sn into ZnO ETL enhanced the PCE of P3HT:PCBM-based OSCs almost by 340 % from 1.01 % (undoped device). The increase in the performance is attributed to the inclusion of the Sn in the ZnO layer. This is advantageous to optimizing charge dissociations, mobility, and collection which resulted in the PCE improvements due to enhancement of V_{oc}, J_{sc}, and FF. To understand the mechanism behind those solar cell parameters increment, properties such as optical and electrical, properties of pristine and Sn-doped ZnO ETL films were systematically studied. In this regard, lower recombination due to defect suppression, uniform distribution of Sn in ZnO ETL, improved light absorption, and high electron mobility of the active layer upon the incorporation of 3wt. % Sn was found to play a major role and provided the device with optimized performance.

1.2. Statement of the problem

In the OSCs device, the ZnO compact layer prepared by the sol-gel method at low temperature provide a significant potential for good quality ETL due to its good characteristics i.e. absence of pinholes, ease of preparation, thickness controllability, and low-temperature processability. But

the ZnO films prepared at low temperature is susceptible to lower charge mobility and electrical conductivity which leads to depreciation in photovoltaic performance. To mitigate these issues Sn was incorporated as a dopant into ZnO ETL so that Sn^{2+} replaces some of the Zn^{2+} ions without affecting the crystal structure of the host due to their comparable ionic radius. Moreover, Sn-doped ZnO as ETL in P3HT:PCBM-based OSCs has not been reported so far. This work paves the way for further improvement in the performance of this blend solar cell by integrating it with Sn-doped ZnO as ETL.

1.3 Objectives

1.3.1 Main objective

The main aim of the present work is to improve the photovoltaic performance of the P3HT-based OSC by developing Sn-doped ZnO ETL films by varying the concentration of Sn in the ZnO structure.

1.3.2 Specific objectives

To achieve the goal of this study, the specific objectives can be summarized as below:

- To synthesize undoped and Sn-doped ZnO by sol-gel method, with various concentrations of Sn i.e. 1 %, 2 %, 3 %, and 5 % by weight which is followed by ETL deposition on ITO substrate by spin coating.
- To characterize the fabricated pristine and Sn-doped ZnO films using Optical spectroscopy, current-voltage (I-V), and X-ray diffractometer (XRD).
- To fabricate and characterize the performance of Sn-doped ETL-based P3HT:PCBM OSCs.
- To determine the electron mobility enhancement that will be obtained in the Sn-doped ETL-based OSCs.

1.4. Significance of the study

With increasing global energy demand, the need for efficient and clean energy sources has become a hot issue. Global energy consumption has more than doubled over the last forty years and in 2015 was approximately 18.5 Terawatt years per year (Sutton, 2018). With the rapid increase in global energy consumption, it is predicted that coal, oil, and natural gas-based world energy are

growing by an average of 0.6 % per year between 2015 and 2040 (US, 2017). These energy sources however lead to the emission of CO_2, which is a major contributor to anthropogenic greenhouse gas worldwide, resulting in rising global temperature. The majority of Ethiopia's population lives in rural regions, with only a few having access to electricity. Hydropower provides over 96 % of Ethiopia's electricity, while biofuels are used to provide most of the country's energy demands for cooking, heating, and off-grid lighting. Ethiopia, on the other hand, intends to replace these energy sources with carbon-neutral status by 2025 (ETHIOPIA). The development of photovoltaic power generation sources like high-performance solar cell devices which is done in this research work is the best alternative to play an important role to mitigate the worldwide issues mentioned above and helping the wide population in Ethiopia to get electric power from solar energy. Moreover, this work would help to get OSCs device without the need of controlled environment such as glove box which add extra cost to the device.

1.4. Scope of the study

The work presented in this thesis serves to establish four main points. First, Sn-doped ZnO was synthesized by room temperature sol-gel method for the electron transport layer and a blend of P3HT and PCBM as an active layer was prepared. Secondly, the synthesized solution of ZnO was spin-coated on ITO glass substrate and annealing on the hot plate in the air which was followed by spin coating of the active layer solution on it and HTL and Al deposition using a vacuum thermal evaporation to get the final device structure; ITO/ZnO(undoped and doped)/P3HT:PCBM/MoO_3/Al. Third, the synthesized component such as undoped and Sn-doped ZnO ETL and photon absorbing layer deposited on ETL were subjected to X-ray powder diffraction (XRD), Ultraviolet-Visible (UV-vis) spectroscopy, and Photoluminescence (PL) spectroscopy, Raman Spectroscopy (RS) and Current-Voltage (I-V) characterization techniques. Fourthly, current density-voltage (J-V) characteristic measurement of all devices with ZnO without and with Sn at a different concentration under illumination for photovoltaic performance evaluation. Finally, electron-only device fabrication with structure ITO/ZnO (undoped and doped)/P3HT:PCBM/Al followed by current density-voltage (J-V) characteristic measurement under dark conditions to obtain the electron mobility of the active layer.

CHAPTER TWO

2. LITERATURE REVIEW

2.1 Organic Solar Cells

2.1.1 Basic Working Principles

This Section provides a clearer grasp of the basic operating principles in BHJ OPV devices for a more in-depth analysis of the OPV. An active layer made up of electron-donating and -accepting materials, referred to as donor (D) and acceptor (A),respectively is sandwiched between two electrodes, one of which must be transparent. Indium tin oxide (ITO) and other transparent conductive oxides (TCO) are commonly utilized. To improve the performance and stability of the BHJ OSCs, interfacial layers such as the hole transport layer (HTL) and an electron transport layer (ETL) are routinely applied between the anode-photoactive and cathode-photoactive interfaces, respectively (Rafique, Abdullah, Sulaiman, & Iwamoto, 2018). To ensure Ohmic connections, these transport layers must match the HOMO level of the donor and the LUMO level of the acceptor in the active layer.

The operation of BHJ OPV devices under illumination can be divided into five steps, as shown in Figure 1: light absorption with exciton formation, exciton diffusion to the donor/acceptor interface, exciton dissociation into free-charges, free-charges transport through the donor or acceptor phases to the electrodes' interface, and free-charges collection at the electrodes (Bolognesi, 2013). After saying this now let me explain in detail each process.

1. Light absorption with exciton formation

The essential requirement for any PV device is that solar light is well absorbed by the active layer (i.e., the majority of the solar spectrum reaching the Earth's surface should be gathered). Since each polymer absorbs a small range of visible light, and the ones used in BHJ solar cells often have little or low absorption in the low energy side of the solar spectrum, this is a problem that has yet to be overcome in organic PV (Deibel & Dyakonov, 2010). It's worth noting that light absorption is limited to the donor material because the absorption coefficient and spectral coverage in the visible region of traditional electron-accepting organic materials are often substantially lower than those of their electron donor counterparts, the dominant light absorber in BHJ OPV devices is

almost always the organic electron donor material (Blom, Mihailetchi, Koster, & Markov, 2007; Rafique et al., 2018). The incident photons pass through the device and reach the photoactive layer, which efficiently absorbs light. Depending on the absorbance of the donor and acceptor, as well as the energy/wavelength of the photon, incident photons may be absorbed by the active layer(Deibel & Dyakonov, 2010). A Frenkel-type exciton is formed when a photon is absorbed, that is, an exciton that is tightly confined by Columbic contact due to the low dielectric constant of organic materials (r = 2–4)(Gehrig, 2015; Scharber & Sariciftci, 2013). An electron is excited from the highest occupied molecular orbital (HOMO) to the lowest unoccupied molecular orbital (LUMO) when photons are absorbed (LUMO). To form electron-hole pairs or excitons, the offset between the donor (LUMO) and acceptor (LUMO) must be in the range of 0.1–1.4 eV (Deibel & Dyakonov, 2010). The optical absorption coefficient of D and A in the film is strictly correlated to their molar absorptivity or molar extinction coefficient (the intrinsic capacity of light absorption by a single molecule), density (number of molecules per volume unit), and absorption cross-section, determines the efficiency of light absorption (the orientation of the absorbing molecules comparing that of the incident light electromagnet field(Bolognesi, 2013; Sharenko et al., 2013).

2. Exciton diffusion and charge dissociation

The excitons must diffuse to the donor-acceptor interface, where there is enough potential energy drop to split them into free charge carriers, such as electrons and holes(Mayer, Scully, Hardin, Rowell, & McGehee, 2007). The exciton is allowed to diffuse to the D/A interface dissociation sites where the exciton is separated into free charges and the exciton, which is mostly produced in the D phase, diffuses as long as there are no geminate recombination processes between the electron and hole that make up the exciton(Bruder, 2010). Due to the shorter lifetime of excitons in most conjugated polymers, diffusion lengths are limited to a few nanometers (less than 20 nm), which is much less than the optical absorption pass length (100–200 nm). Excitons must consequently be created within their diffusion length (LD) to generate charge efficiently (Scharber & Sariciftci, 2013). The hole remains on the donor molecule after exciton dissociation, while the electron is transported to the acceptor molecule.

3. Free charge carriers transport

After the exciton dissociation into free charge carriers, the charges should be transported towards the respective electrodes as shown in Figure 1(b). In comparison to the recombination of Frenkel

excitons, the recombination rate after charge carriers spatially separated is lower because each charge carrier rests on two different molecules (Deibel & Dyakonov, 2010). The degree of order of the molecular species in the BHJ film affects the charge transport mechanism in organic semiconductors. Two types of charge transport systems can be distinguished: hopping transport or band transport (Bolognesi, 2013). In inorganic semiconductors, where charges are delocalized over the electronic states that make up the semiconductor's conduction band, band transport is an atypical transport mechanism, whereas, in amorphous organic semiconductors, the characteristics hopping transport mechanism occurs when conductive electronic states are in more localized rather than consisting of electronic bands. The hopping charge transfer mechanism frequently prevails because the semiconducting organic films utilized in BHJ OPV devices are generally amorphous or semi-crystalline so charge carriers are transferred from one localized state to the other (Baranovskii, Cordes, Hensel, & Leising, 2000; Pivrikas, Sariciftci, Juška, & Österbacka, 2007). Because of the Fermi level difference between the electrodes, an internal electric field induces the transit of free charge carriers towards their respective electrodes (Zhou, Eck, & Krüger, 2010). The intrinsic morphological properties of the D and A phases, characterized by finely intermixed and distorted domains of the two materials, are another major limiting factor in the charge transfer of free charges from the exciton dissociation sites to the electrodes in BHJ OPV devices.

4. Charge collection at the electrodes

Charge carriers created by photons that do not recombine are typically extracted from the photoactive layer and delivered to the electrodes. To maximize charge extraction, the potential barrier at the photoactive layer/electrode contact must be lowered (Deibel & Dyakonov, 2010). The work function of the cathode should be lower than the $LUMO_A$ level, and the work function of the anode should be greater than the $HOMO_D$ level, for free charges to be collected at the corresponding positive and negative electrodes (Figure 1b). The difference between the electrode's WF and the $LUMO_A$ or $HOMO_D$ energies determines whether the related electrodes have ohmic or blocking contacts for charge injection i.e. if the WFs match well as described, then the contacts are said to be Ohmic contacts (Rafique et al., 2018). Whenever the electrode/organic contact is non-ohmic, the interfacial energy level alignment between the organic frontier orbitals and the WF of the contacts may result in electrical losses for the device, whereas ohmic contacts should result in more efficient charge collection at the electrodes(S.-S. Sun & Dalton, 2008).

To summarize, after charge separation, charge carriers are extracted by a bicontinuous network of percolation routes connecting the donor and acceptor domains to their respective electrodes. Finally, a variety of factors influence total efficiency, including (Jaumot, Gargallo, De Juan, & Tauler, 2005): i) fraction of absorbed photons, ii) exciton quenching efficiency, iii) charge separation/dissociation efficiency, iv) charge transport and extraction efficiency. Each of the above-mentioned processes in the charge generating process must be carefully optimized to ensure optimal photovoltaic performance.

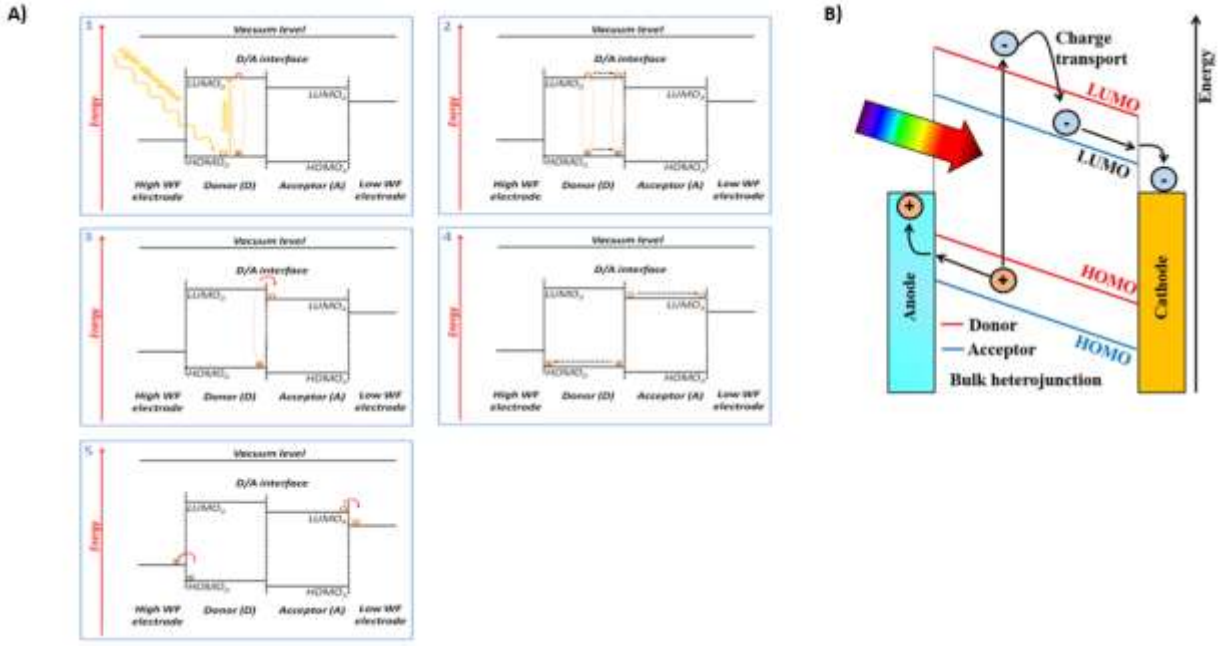

Figure 1. *(a) Charge generation mechanism in an organic solar cell including from light absorption and exciton generation to (1) to charge collection at respective electrodes (5) and (b) Band diagram of the photocurrent generation mechanism in a BHJ solar cell (Bolognesi, 2013; Rafique et al., 2018).*

2.1.2 Photovoltaic parameters

The ability of an organic solar cell to convert light to electrical energy is reflected in the current density, J_{sc} as a function of the voltage,V under illumination conditions, and the photovoltaic parameters that determine the efficiency of the solar cell can be extracted from these curves as shown in Figure 2a. These photovoltaic parameters are summarized below

2.1.2.1. Short circuit current density (J_{sc})

A short circuit current is the current that flows through a solar cell when the applied voltage is zero or in other words, it represents the number of charge carriers generated and finally collected at the respective electrodes at zero applied potential(Fung & Choy, 2013). J_{sc} is primarily determined by the D material's ability to absorb light and form excitons, which is determined by the material absorption coefficient and band gap, as well as the exciton diffusion at the donor/acceptor interface, which varies with the exciton diffusion lengths of the materials. Moreover, in the BHJ film, J_{sc} is influenced by carrier mobility in the D and A phases, as well as their electrical conductivity and shape. Since the current is roughly proportional to the illuminated area, the current density J is often used instead of I_{sc} (and correspondingly J_{sc} instead of I_{sc}).

2.1.2.2. Open circuit voltage (V_{oc})

This is the voltage when there is no current flowing through a solar cell under light illumination or is the measure of the maximum of the voltage that a solar cell can extract for an external circuit. Because of several loss mechanisms, the photogenerated charge carrier is canceled out in this scenario (Tegegne, 2018). For traditional single-junction inorganic solar cells, Voc is mainly determined by the band gap of the absorbing semiconductor, although being limited by the recombination of charges through radiative processes (Shockley & Queisser, 1961) whereas, in BHJ OPVs in which charge separation at the D/A interface occurs very efficiently the energy difference between the acceptor LUMO and the donor's HOMO determines the open-circuit voltage primarily (Keivanidis, Howard, & Friend, 2008). Furthermore, depending on the D/A blend morphology as well as the morphology and nature of the electrode, experimental Voc values may differ from those inferred from that difference (Blakesley & Neher, 2011).

2.1.2.3. Fill factor (FF)

The fill factor is defined as the ratio of the maximum power obtainable to the product of open-circuit voltage and short circuit current or the measure of the squareness of the J-V and is given by the equation:

$$FF = \frac{V_{max} \times I_{max}}{V_{oc} \times J_{sc}} \qquad (1)$$

Where V_{max} and I_{max} are the voltage and the current at the maximum power (P_{max}) point respectively.

The FF is limited e.g. by the field dependence of charge generation or extraction. If there is no field dependence in the organic solar cell, the FF might approach a value of 1. Moreover, the FF is also limited by unbalanced charge transport (Zhou et al., 2010) i.e. very different hole and electron mobility because unbalanced charge transport results in a space charge limited photocurrent which in turn limits the FF. The FF is also related to the solar cell quality and its electrical resistances i.e. Series resistance (R_s) and shunt resistance (R_{sh}) (see Figure 2(b)). Larger R_s and lower R_{sh} result in reduced FF and, as a result, lower cell efficiencies. This issue can be avoided by the precise choice and processing of the buffer layers and electrodes which lower the contact resistance, thus the Rs and while the improvement of the BHJ morphology, as well as the control and tuning of the energy and kinetics involved in the charge separation process, lowering shunt currents bypassing the D/A interface, thus increasing R_{sh} (Rafique et al., 2018). Moreover, these two resistors significantly alter the real I-V behavior of a BHJ OPV so that the voltage V lowers over the R_s whereas R_{sh} resistance adds the current to the cell output current. The R_{sh} accounts for any leakage current and this leakage can be occurred due to some defects in the preparation of the device (Tegegne, 2018).

2.1.2.4. Power conversion efficiency (PCE)

The ratio of a solar cell's electrical output to the incident light power to which it is exposed is known as solar cell power conversion efficiency. This is computed by dividing the maximal output power density (P_m, in W/m^2) by the incident light irradiance (P_L, in W/m^2), as follows:

$$\eta = \frac{P_{out}}{P_{in}} = \frac{FF(V_{oc}\, x\, J_{sc})}{P_{in}} \qquad (2)$$

Where P_{out} and P_{in} represent the output and input power respectively.

2.1.2.5. Maximum power (P_{Max})

This is the maximum electric power produced by the OPV cell under illumination and the maximum of the power curve (P_{max}) and corresponds to the maximum power point (MPP) in the I -V curve (see Figure 2)

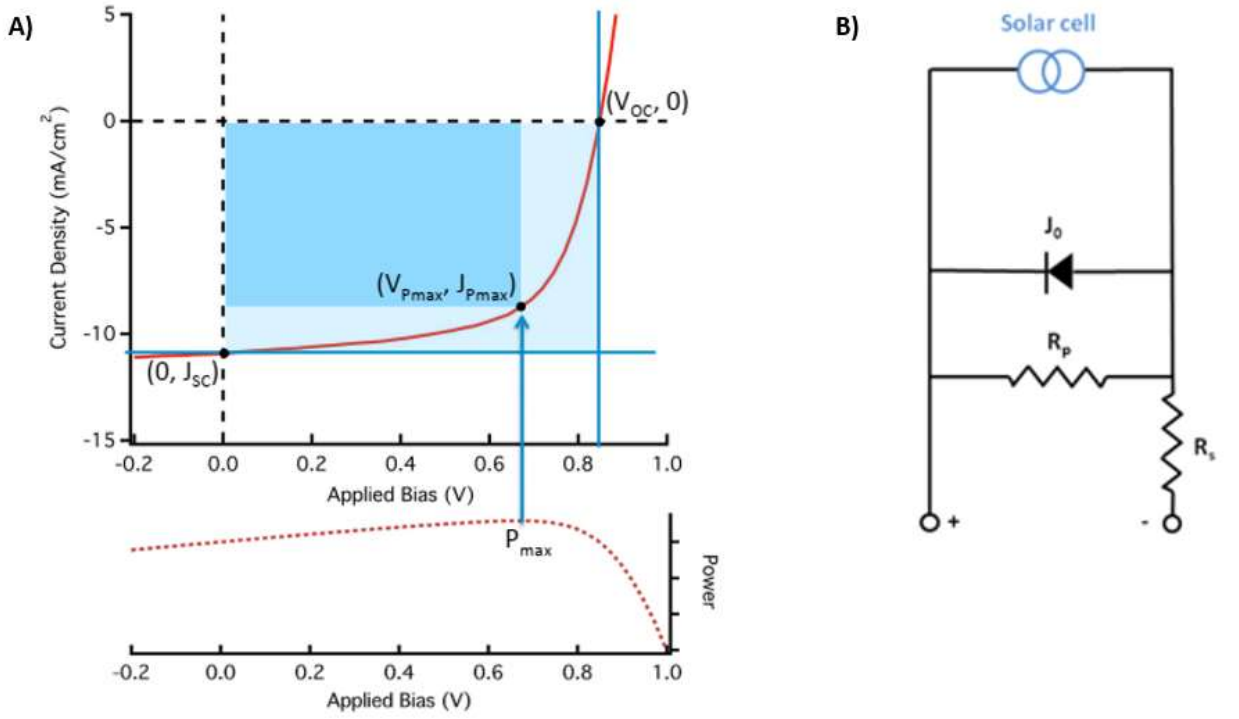

Figure 2. *(a) Device properties depicted by a current-voltage curve for a solar cell (b) Equivalent circuit of a solar cell. The Rsh resistance accounts for leakage current and RS is due to any hindrance to the current flow in the solar cell (Braid, 2016; Gehrig, 2015).*

2.1.3 Device configuration in bulk heterojunction solar cells (BHJSCs)

In OSCs, there are two device configurations namely, standard and inverted geometries of the device which are shown in Figure 3. As already mentioned in the introduction, the normal structure typically consists of a transparent electrode (ITO) as an anode at the bottom for the hole collection, followed by deposition of hole transport layer (HTL) as anode buffer or interfacial layer and then a thin layer of active material which is followed by deposition of electron transport layer (ETL) as a cathode buffer or interfacial layer, finally a top metal electrode as a cathode for the electron collection(Figure 3a). The same thing applies to inverted device structures except for changing the position of ETL and HTL. In the inverted structure (Figure 3b), the role of the electrodes are swapped; thus, the electrons are collected by the bottom transparent electrode and the holes by the

top metal electrode whereas in the normal structure holes are collected in the bottom electrode, and electrons in the top electrode.

Because of the reversed collection, the top electrode's work function must be high enough to match the donor's highest occupied molecular orbital (HOMO) energy level, while the bottom electrode's work function must be low enough to match the acceptor's lowest unoccupied molecular orbital (LUMO) energy level (Facchetti, 2013). While the top metal electrode requirement can be easily met by selecting high work function metals such as gold or silver, the correct selection of the bottom electrode is more difficult in fact, the most commonly used transparent metal oxides, such as ITO or FTO, and have high work functions that do not match well with the acceptors' LUMO level (Rafique et al., 2018). The energy levels are matched by changing the bottom electrode by depositing a thin layer of suitable electron-conducting (hole blocking) materials, such as ZnO, which is the most extensively used and transparent to visible light. The Normal device structure is with consequent problems of device stability in air and/or moisture due to the easy oxidation of the low WF metal. Due to its acidity, PEDOT:PSS, for example, might readily damage the ITO electrode, impacting device stability over time(Bolognesi, 2013). Moreover, the employment of an air-sensitive ETL in a traditional device structure makes it impossible to execute the fabrication process in air, necessitating the use of thermal evaporation techniques under vacuum, boosting the complexity and fabrication expense of these devices. devices, the employment of an air-sensitive ETL in a traditional device structure makes it impossible to execute the fabrication process in air, necessitating the use of thermal evaporation techniques under vacuum, boosting the complexity and fabrication expense of these devices(H.-C. Chen et al., 2015). Inverted device designs also employed in this thesis, on the other hand, have recently gained a lot of attention due to their greater stability as compared to conventional devices, the higher WF metal electrode (such as Au and Ag) in this configuration is more resistant to air and moisture oxidation, overcoming one big hurdle for possible widespread application of Polymer solar cells, boosting overall cell durability (Sasajima, Uesaka, Kuwabara, Yamaguchi, & Takahashi, 2011). Moreover, Inverted device structures have been devised to tackle the problems related to the air sensitivity of ETL in a traditional device structure, reversing the transport direction of electrons and holes by using a metal with a high work function as the anode on top of a device with ITO as the cathode at the bottom(He et al., 2012; Lloyd et al., 2009). Furthermore, in the case of inverted solar cells, the high-work-function metal anode, such as Ag, can be prepared using either coating or printing technology,

both of which are compatible with all solution processing and thus can greatly simplify the fabrication process and reduce solar cell manufacturing costs (Girotto, Rand, Steudel, Genoe, & Heremans, 2009; Krebs, 2009). Another advantage of inverted geometry over normal geometry is that it allows for more flexibility in the construction of multi-junction or tandem solar cells [13, 25]. The inverted device configuration is also more advantageous than the standard configuration due to the vertical phase separation mechanism, which characterizes the P3HT prone to collect on the electrode top and the fullerene derivative on the bottom (L. M. Chen, Hong, Li, & Yang, 2009).

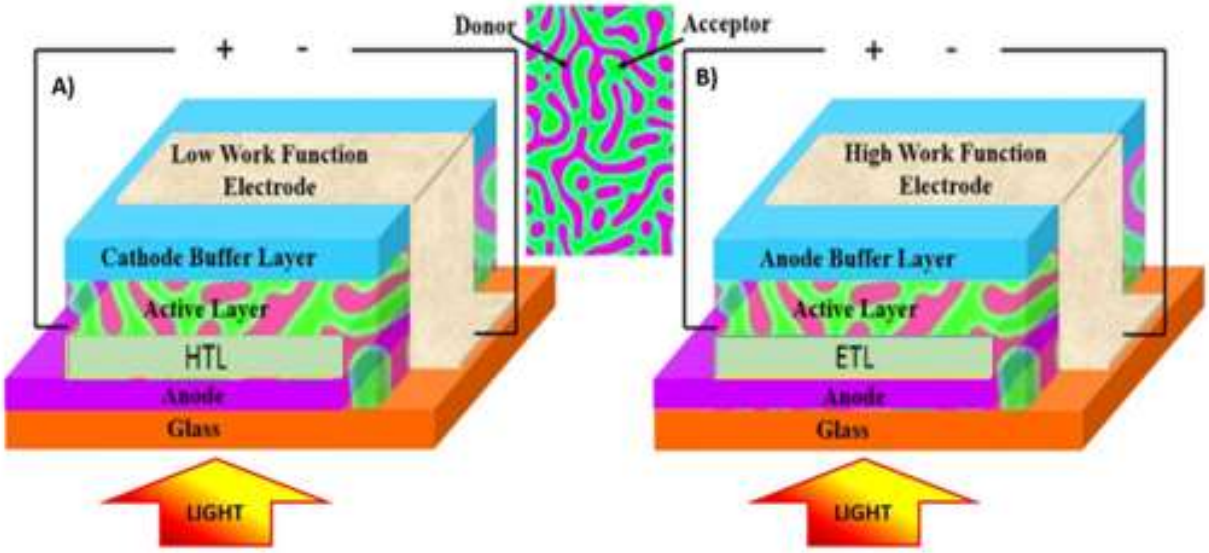

Figure 3. *Schematic illustration of device structures of (a) conventional and (b) inverted OSCs with bulk heterojunction active layer (Rafique et al., 2018).*

It has been reported by Brabec group's using the outstanding achievements obtained by numerous research groups, through device engineering of normal or inverted structures and the use of new polymers or continuous exploring of high-performance materials, the state of the art PCEs of OSCs have been dramatically improved (Figure 4). The study of the high PCE, stability, and the roll-to-roll process has become three major directions in polymer solar cells (You, Dou, et al., 2013). The inverted Polymer solar cells appear to be the greatest contender for high efficiency, good stability, low cost, and compatibility with the existing roll-to-roll technology.

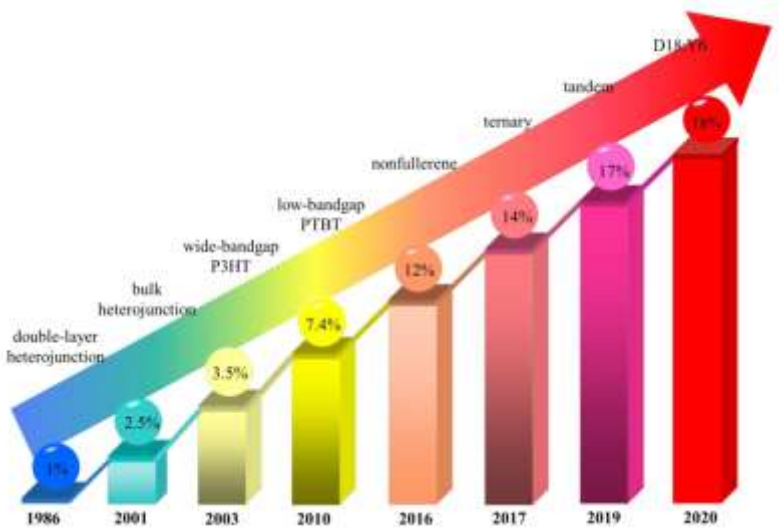

Figure 4. *The progress of PCE in OSCs (Xu et al., 2020).*

2.1.4 Charge mobility measurement in OSCs

The electrons are confined in the PCBM phase after photo-induced electron transfer at the donor/acceptor interface, while the holes stay in the PPV polymer chains. The free electrons and holes must then be delivered to the electrodes via percolated PCBM and Polymer (P3HT) routes to produce the photocurrent (Valentin Dan Mihailetchi, 2005). As a result, understanding the optoelectronic properties of bulk heterojunction solar cells requires an understanding of electron transport in PCBM and hole transport in Polymer. The disparity between electron and hole mobility in the P3HT:PCBM blend is reduced, often by a factor of ten, resulting in more balanced transport, requiring direct measurement of hole and electron mobilities in the blend as employed in the operational device(Valentin Dan Mihailetchi, 2005).

Charge transport is crucial for optimum device performance in organic semiconductors. Under high irradiances, efficient, balanced charge transfer in OPVs reduces current losses from recombination and series resistance losses (Lenes, Morana, Brabec, & Blom, 2009; Valentin D Mihailetchi & Xie, 2006). A variety of procedures were used to determine charge mobility. The steady-state space-charge limited current (SCLC) approach and the transient methods, which

included time of flight (TOF) (Kemerink et al., 2003), dark-injection transient current (DITC), and charge extraction by linearly increasing voltage, were used (CELIV).

Because the dark current is space-charge limited (SCL), the mobility can be determined directly from J_D-V measurements. In blend devices, however, the existence of Ohmic contacts at both interfaces causes an SCL current, which is a mix of electron and hole current (Valentin Dan Mihailetchi, 2005). As a result, to measure the SCL current of only one type of charge carrier, a substantial injection barrier must be used to suppress the other, resulting in an electron- or hole-only device. Although many scientists think that the SCLC technique is the most adaptable for material benchmarking applications, some high electron-mobility materials may have problems with electron injection (Steyrleuthner et al., 2010; Wetzelaer, Najafi, Kist, Kuik, & Blom, 2013).

A hole-only or electron-only diode device construction is required for SCLC measurements. At least one electrode must effectively inject the desired charge carrier, while the other must prevent opposite-polarity charge carriers from being injected. When a voltage is given to the diode, a unipolar charge is injected into the semiconductor film, causing space charge to build up (Mott, 1940). The space charge is sufficient to diminish the electric field at the injecting contact over time (longer than the carrier transit time), and the quantity of charge inside the device saturates. Only enough new charge is injected to replace the charge that has been removed at the opposite electrode. The steady-state current density (J_{SCLC}) is a function of the applied voltage V, the film thickness d, the film permittivity e, and the steady-state charge-carrier mobility, assuming uniform charge-carrier mobility (equation 8). This equation has the advantage of being able to match a wider range of I–V curves, but it is subject to the following assumptions:

Charge injection is efficient: The injecting electrode must be able to inject sufficient current into the organic semiconductor material to keep the current bulk-limited instead of interface-limited. This is usually accomplished by utilizing an electrode with a work function aligned to the semiconductor's intended HOMO or LUMO level and a low contact resistance (ZB Wang, Helander, Greiner, Qiu, & Lu, 2009).

Devices are unipolar: Electron injection from the collecting electrode must be inhibited for hole-only devices, and vice versa for electron-only devices. Comparing different electrode combinations can confirm this.

Charge trapping: Organic semiconductors have traps as a result of instability, contamination, flaws, or deterioration. They've been discovered as a particular problem in polymer electron transport (Nicolai & Kuik, 2012). A fraction of charge carriers will be caught in a system with charge traps, while the rest will be free to move.

No domination of Series resistance: When the current is strong, external series resistances (for example, from thin-film electrode materials used for contacting) can diminish the voltage dropped across the semiconductor film. At high voltages, the current-voltage curve becomes linear, indicating this. This is especially true when attempting to characterize thin coatings of high mobility materials (Blakesley et al., 2014).

2.2. Hole and Electron Transport Layers in Organic Solar Cells

In OSCs and other solar cells (SC) systems, the five components that play a crucial role in device operation include meta based cathode (metal contact), hole transport layer (HTL), absorber layer (the perovskite layer), an electron transport layer (ETL), and transparent conductive oxide (TCO) (Roy, Kumar Sinha, Tiwari, & Khare, 2020). Among these components, the ETL and HTL along with the photon absorber layer play significant roles in SC operation. The active material in both regular and inverted devices serves the same purpose: to absorb photons and transform them into free charge carriers. However, to produce satisfactory results, a BHJ must include both an HTL and an ETL. By improving charge extraction efficiency from the active layer over metal/organic interfaces, the employment of an electron transport layer (ETL) and a hole transport layer (HTL) between the BHJ and electrodes increases device performance dramatically(Braid, 2016).

2.2.1. Hole Transport Materials (HTMs)

The HTL collects or extracts the hole from the absorber layer but it has to block electrons. It acts as a physical/energetic barrier between the active layer and ETL by hindering the transfer of electrons (Pitchaiya et al., 2020). Hole transport materials (HTMs) play an important role in the overall solar cell device performance and the researchers must take into account the following prospects for the introduction of new HTMs. It should possess suitable energy levels, providing the driving force for charge transfer, which means the highest occupied energy level, i.e., the highest occupied molecular orbital (HOMO) energy levels of the selected HTMs must be slightly above that of the BHJ materials (Litzov & Brabec, 2013). Moreover, it should act as a barrier

between the anode and active layers to block electrons from entering the anode. A good HTM needs to have four major requirements including high hole mobility, optimal HOMO energy level, good solubility and film-forming properties, and low cost (Ansari, Qurashi, & Nazeeruddin, 2018). From the standpoint of interfacial contact, Proper modification of the anode electrode by inserting an HTL is an effective and simple method to drastically improve the PCE of the OSCs. In any case, the inclusion of an HTL layer between the organic active layer and the top metal electrode is required to gain high performance from OSCs; otherwise, the device would work poorly or not work at all (Servaites, Ratner, & Marks, 2011).

The HTL can be classified as organic, inorganic, and carbonaceous. The organic-based HTL includes a long-chain polymer and small molecules, which are nearly polymeric-based. The inorganic HTL includes Nickel-based, copper-based, p-type semiconductors and transition metal HTMs (Pitchaiya et al., 2020). However, the most commonly used HTLs in BHJ SCs are polymers, like PEDOT:PSS, or metal oxides, like MoO_3, V_2O_5, WO_3, NiO (Lattante, 2014).

PEDOT: PSS is the most widely used HTL in standard geometry BHJ solar cells because of its high work function (which closely matches the HOMO level of commonly used donor polymers), high transparency in the visible range (greater than 80%), good electrical conductivity, and ability to reduce ITO surface roughness while increasing work function (Carter, Angelopoulos, Karg, Brock, & Scott, 1997). However, because PEDOT: PSS is very hydrophilic when deposited as the HTL onto hydrophobic organic layers in inverted devices, poor film morphology, and electrical characteristics have been found (Ionescu-Zanetti, Mechler, Carter, & Lal, 2004; Kemerink, Timpanaro, De Kok, Meulenkamp, & Touwslager, 2004). The detail of PEDOT: PSS and other organic HTMs are available at (Xu et al., 2020). Figure 5 shows the flow chart on the classification of the HTMs.

It has been demonstrated in the past that high work-function metal oxides and molybdenum trioxide (MoO_3) might be suitable alternatives for PEDOT: PSS. Nowadays, MoO_3, with its large bandgap between 2.9 and 3.1 eV and high work function of 5.5 eV (Ren, Sun, Cui, & Li, 2018) is widely under use as the most suitable HTL in OSCs. Both inverted and regular OLEDs benefit considerably from a thin HTL of (MoO_3) (Meyer et al., 2007; F. Wang, Qiao, Xiong, & Ma, 2008). Chen and coworkers demonstrated that MoO_3 improved the overall efficiency of a BHJ ISC with

both a P3HT:PCBM active layer and a nanocrystalline TiO_2 ETL in early 2008 (C. Tao et al., 2008). To achieve the same performance as devices employing Ag or Au, an increased thickness of the evaporated MoO_3 layer is necessary using Al as the top electrode. This is due to the chemical reaction between Al and MoO_3 during the evaporation process, which resulted in the formation of a MoO_2 species due to MoO_3 reduction according to this literature (C. Tao et al., 2008). The MoO_3 thickness dependence of efficiency has been explained by the works reported by Zheng et al. (Yin, Zheng, Chen, & Cai, 2013) and by Wantz and coworkers (Chambon et al., 2012), they demonstrated that when the thickness of the MoO_3 layer was in the region of 10–20 nm, basic device characteristics remained nearly same, but when the thickness was reduced to 5 nm, both V_{oc} and FF dropped. Moreover, they also found that a decrease in the thickness of the MoO_3 layer was followed by both an increase in the series resistance and a drop in the shunt resistance when the thickness of the MoO_3 layer was reduced.

To sum up, the HTL can increase the WF of the ITO anode while lowering the interfacial energy barrier between the anode and the active layer, allowing for the creation of ohmic contact between the ITO anode and the active layer, the HTL can block electrons and minimize interfacial charge recombination, the HTL can physically change the surface of the ITO anode, passivate surface imperfections and pinholes, and reduce leakage current, Finally, the HTL can influence the active layer's shape and absorbance, as well as the PCE of OSCs (Bilby, Frieberg, Kramadhati, Green, & Kim, 2014; Tu et al., 2016; Yin et al., 2013).

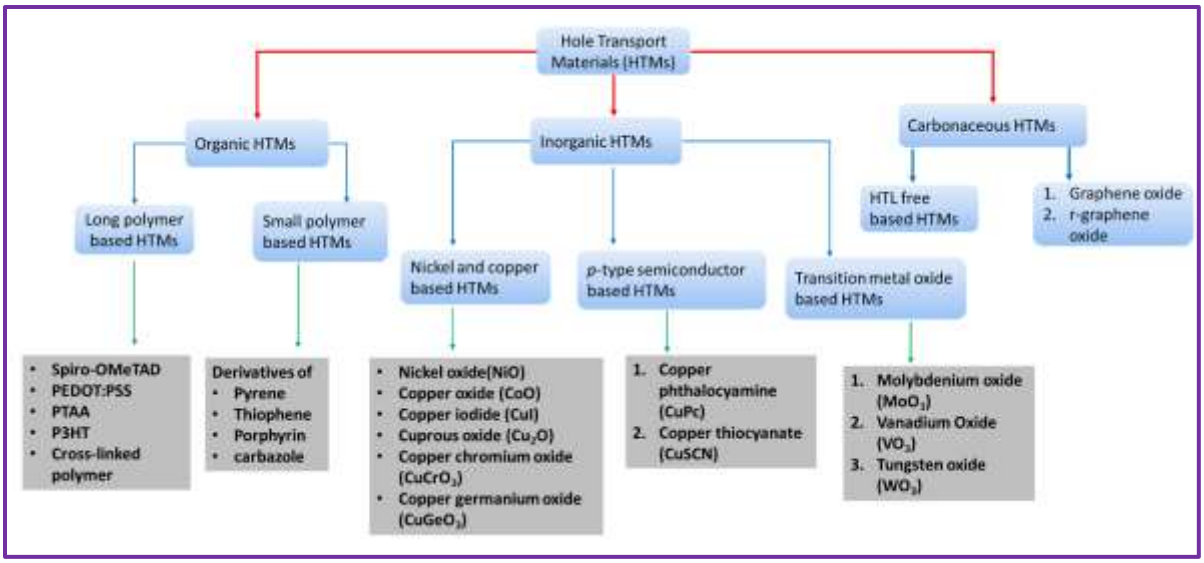

Figure 5. *Flowchart illustrating the classification of hole-transporting materials (HTMs)(Pitchaiya et al., 2020).*

2.2.2. Electron Transport Materials (ETMs)

The function of ETL is the extract of electrons from the absorber layer and transport them towards the anode and it must block holes. The necessary condition for materials to serve as ETL are: the uppermost occupied energy level, HOMO, and the lower unoccupied energy level, LUMO should be higher and lower, respectively than that of the active layer, high transmittance of light over a wider wavelength range to enable high fraction of light with sufficient energy to reach the active materials in the case of inverted BHJ solar cell devices (Mahmood, Sarwar, & Mehran, 2017). To improve electron extraction from the BHJ layer and lower V_{oc} loss, an ETL molecule's highest occupied molecular orbital (HOMO) must have a deeper value than the active layer's valence band to prevent holes from moving to the cathode and limit current leakage. Furthermore, ETLs with high electron mobility have a better ability to transfer electrons to the cathode, resulting in low series resistance.

To use ITO as a cathode, its work function must be set toward higher energies to increase its electron affinity, which is commonly achieved by employing the suitable ETL, and a lower energy metal (such as Ag or Au) should be used as the metal electrode (Bolognesi, 2013). Semiconducting metal oxides, low WF metals and metal salts/complexes, polymers and small molecules, carbon-based materials, and other ETL materials have all been developed to improve device performance

(Agnihotri, Sahu, & Tiwari, 2017). In BHJ-based OSCs, various materials such as TiO_2, SnO_2, SiO_2, ZnO, and phenyl-C61-butyric acid methyl ester (PCBM) can be used as ETL.

The most widely used ETL material was TiO_2 which possesses a wide band gap(3.2eV) and this large band gap prevents the absorption of light energy and low chance for the generation of the hole during operation so that electron-hole recombination is reduced. Even though porous crystalline TiO_2 is the standard charge transport layer in dye-sensitized solar cells, it is not well suited as the ETL in BHJ ISCs due to the tough and challenging deposition of a uniform and homogeneous layer on conventional ITO substrates (Baglio, Girolamo, Antonucci, & Aricò, 2011). Peng et al. (R. Peng et al., 2013) reported TiO_2 ETL in inverted solar cells (ISCs), demonstrating that the device's overall power conversion efficiency is highly dependent on the crystalline structure of TiO_2. Furthermore, the interface between TiO_2 and the active material has an optimal morphology and interaction when the film has a well-defined morphology (homogeneity of nanoparticle shapes and distribution) and maximum crystal size of about 50 nm, favoring both exciton dissociation and charge separation, with improved FF (less charge recombination and improved charge transport through the inorganic layer). Inverted devices made of amorphous or crystalline TiO_x (typically formed using the sol-gel technique (Litzov & Brabec, 2013)) have the same efficiency range as ZnO (Hadipour, Müller, & Heremans, 2013; Litzov & Brabec, 2013). The physical and chemical properties of an amorphous TiO_x layer can be tuned to improve the performance of devices that use it. The limitation of TiO_2 is its small electron mobility (0.1 4 cm^2 V^{-1} s^{-1}) compared to the ZnO ETLs (Ameen, Akhtar, Shin, & Nazeeruddin, 2018) and this in turn hinders the electron extraction from the active layer to the ITO electrode timely and leads to charge accumulation near the interface so that further extraction of charge is greatly affected.

Tin oxide (SnO_2) is a very transparent conducting substance that is nontoxic, plentiful, and has a broad bandgap (3.6 eV)(Z. Chen et al., 2014). SnO_2 has been widely used as an effective ETL for optoelectronic devices, particularly perovskite solar cells, because of its remarkable electrical and optical characteristics (H. Tao et al., 2018). Tin oxide has higher inherent mobility than other n-type oxides, which allows for more efficient carrier movement. Solution-processed SnO_x films and SnO_2 NPs have recently been produced as ETLs for inverted OSCs (Bob, Song, Chen, Xu, & Yang, 2013). Previous research has revealed that inverted OSCs utilizing SnO_2 have not only free light-

soaking issues but also extremely long-term device stability. Until now, the manufacture of SnO_2 for inverted OSCs has primarily relied on expensive thermal evaporated deposition processes that are usually carried out at a high temperature (500 °C) and high vacuum (S. Yu, Yang, Li, & Zhang, 2016). It is impracticable to fabricate inverted OSCs on flexible substrates at high temperatures above 200 °C. When compared to other n-type oxides, bulk SnO_2 has a higher mobility value, which benefits practically any application that requires efficient carrier transportation. The extraordinarily high mobility values reported in solution-processed tin oxide thin-film transistors have recently highlighted this characteristic (Bob et al., 2013). The PCE of SnO_x ETLs inverted OSCs was comparable to that of TiO_x ETLs based OSCs. Unlike the devices with TiO_x, the OSCs based on SnO_x ETLs without encapsulation were relatively stable even after heat treatment in humid air (Bob et al., 2013). In the next section, a detailed review of ZnO as ETL in OSCs is provided.

2.3. Zinc Oxide (ZnO) Electron Transport Layer (ETLs) in Organic Solar Cells

The type of cathode buffer layer (CBL) material used in inverted polymer solar cells (PSCs), as well as the quality of the interface between the CBL and the BHJ active layer, have a significant impact on device performance (Wan et al., 2011). A ZnO film put between the BHJ active layer and the cathode in inverted PSCs can serve as a CBL to collect and transport electrons while also blocking the reverse flow of holes from the donor polymer to the cathode. ZnO has been the most thoroughly explored material for CBL in inverted PSCs among the materials described above, owing to its acceptable energy levels, strong electron mobility, good transparency, environmental stability, and inexpensive cost (Po, Carbonera, Bernardi, & Camaioni, 2011; Y. Sun et al., 2011; White, Olson, Shaheen, Kopidakis, & Ginley, 2006). The conduction band bottom and valence band top energy levels of ZnO are around -4.4 eV and -7.8 eV, respectively, therefore the band locations allow ZnO to work well for electron collecting and hole blocking (see Figure 6). The valence band top of ZnO, at -7.8 eV, is lower than the polymer donor's highest occupied molecular orbital (HOMO), which is -5.0 eV for P3HT, therefore the reverse flow of holes from the polymer donor to the ITO cathode is stopped by the large energy barrier at the P3HT/ZnO interface leading the ZnO CBL to prevent leakage current from arising at the polymer/ITO interface (Schumann et al., 2011; T. Yang et al., 2010). This phenomenon suggests that inverted PSCs with ZnO CBLs

have been discovered to have significantly better photovoltaic performance than those without. Furthermore, ZnO's relatively high electron mobility makes it a good material for a cathode buffer layer to reduce charge recombination, and its good transparency across the entire visible spectrum benefits lowering optical loss, while the band edge cut-off of ZnO at around 375 nm can block UV light and thus protect organic materials from photo-degradation when exposed to UV light (Schumann et al., 2011; T. Yang et al., 2010). Another advantage of ZnO as a CBL material is that it may be prepared easily using a solution approach and then thermally treated at low temperatures which makes ZnO entirely compatible with all solution roll-to-roll production on flexible plastic substrates, which is a key benefit of polymer solar cells (Jørgensen et al., 2012; Y. Sun et al., 2011). Almost all inverted PSCs manufactured by roll-to-roll manufacturing use ZnO thin layers as the CBL(Krebs, Gevorgyan, & Alstrup, 2009; Krebs, Tromholt, & Jørgensen, 2010; Lilliedal, Medford, Madsen, Norrman, & Krebs, 2010; Søndergaard, Hösel, & Krebs, 2013) are all numbers that can be used to make several different combinations because ZnO has been found as a good material to serve as the CBL in inverted PSCs because of these characteristics and benefits. Although ZnO shows promise as an electron transport layer, electron extraction from typical fullerene electron acceptors into ZnO is limited by natural barriers. The electron affinity of the oxide is much lower than that of the fullerene, as seen in Figure 6 (b). Changing the electron transport layer's work function relative to the BHJ can lower the electron extraction barrier, boosting the device's PCE, V_{oc}, FF, and J_{sc} (Braid, 2016). To effectively modify the work function of a material, one must modify the material itself using most notably substitutional doping and surface modification which will be discussed in the following section.

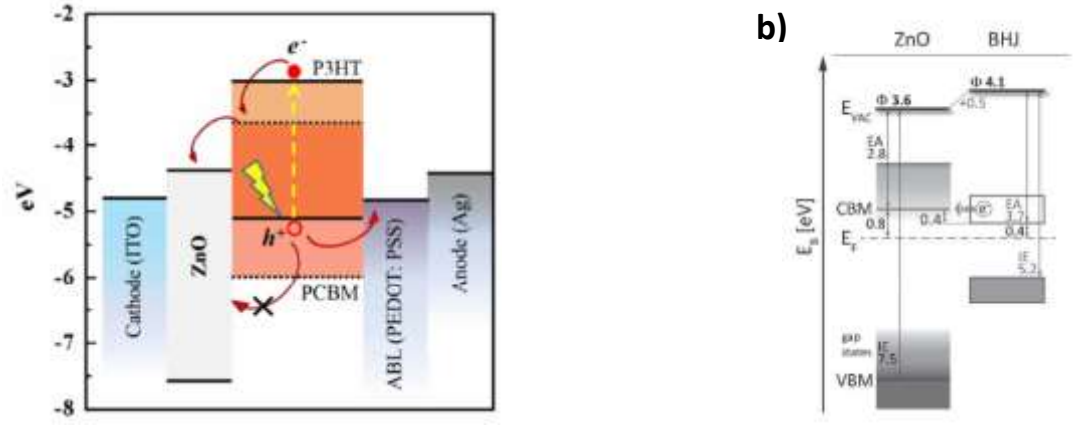

Figure 6. *(a) Schematic illustration of the energy level and the main charge transportation of in inverted PSC with ZnO CBL and P3HT:PCBM active layer (b) Electron extraction barrier of 0.4 eV between the*

electron affinity of PC71BM and the conduction band minimum (CBM) of ZnO (Braid, 2016; Liang, Zhang, Jiang, & Cao, 2015).

2.3.1. ZnO electron transport layers (ETLs) in inverted polymer solar cells (PSCs)

Considering the P3HT:PCBM and other types of organic and inorganic based devices just as a prototypical PV system, many scholars have reported ZnO as the ETL, and PCE is improving from time to time. The mostly reported works on the use of ZnO as ETL in inverted OSCs mainly depend on the design, fabrication, and characterization of ZnO, doped-ZnO, and ZnO-based composite CBLs as well as their surface chemistry and morphology modification for photovoltaic performance enhancement in inverted polymer solar cells (PSCs).

Doping is the common strategy employed in ZnO structure to increase charge collection efficiency and prevent charge recombination owing to charge entrapment by defects or oxygen ions is to properly dope the ZnO layer to enhance the conductivity and other properties of ZnO which in turn improve the photovoltaic performance of inverted solar cells (Litzov & Brabec, 2013; Ohyama, Kozuka, & Yoko, 1998). The thickness of ZnO CBLs in inverted PSCs is typically only a few tens of nanometers to provide high conductivity and so reduce serial resistance and increase device performance (Stubhan et al., 2011), however, the devices' mechanical resilience and protective characteristics against chemical or physical reactions between the active layer and the electrode suffer as a result of the thin CBL.

Alstrup, J., et al.,(Alstrup, Jørgensen, Medford, & Krebs, 2010) doped Al to ZnO to increase the conductivity and quality of ZnO films formed using the slot-die coating process. Since it improves device performances (S.-H. Lee, Kim, Shim, & Park, 2009) and device stability (Lattante, Perulli, & Anni, 2011), lithium fluoride (LiF) has been utilized as an ultra-thin layer beneath the top Al electrode in standard configuration bulk heterojunction solar cells for a long time. Li, J., et al., (Li et al., 2019) reported various concentrations of Cd-doped ZnO (2.5, 5, and 10%) as the ETLs in inverted polymer solar cells built using PTB7-Th:PC71BM as the active layer, and in this research, they recorded that PSCs containing 5% CZO has a short-circuit current (JSC) of 17.15 mA/cm2, a fill factor (FF) of 69.38 %, and a power conversion efficiency (PCE) of 9.28 %. Internal metal ion doping in ZnO can significantly minimize surface charge recombination and increase electron

extraction that leading to improved solar cells performance according to the literature (Li et al., 2019). Yang, Z., et al.,(Z. Yang et al., 2017) utilized and studied Al-doped ZnO (AZO) ETL in the inverted device based on a ternary blend of polymerthieno [3,4-b] thiophene/benzodithiophene (PTB7), [6,6]-phenyl C71-butyric acid methyl ester (PC71BM) and indene-C60-bisadduct (ICBA), demonstrated that the use of ZnO/ AZO nanoparticles improves both short and open circuit current (J_{sc}) and voltage (V), resulting in a recorded power conversion efficiency (PCE) of 8.85 % which is due to the lower work function of AZO than ZnO, resulting in a bigger built-in potential across the organic heterojunction and hence more effective photo-current extraction and larger open-circuit voltages. According to Krebs et al., Al-doped ZnO (AZO) with an Al-to-Zn ratio of 1% can greatly improve the conductivity of the AZO layer, thus improve device performance (Oh et al., 2011) and the strong association between AZO CBL shape and light trapping in inverted PSCs is worth investigating further. Wei, J., et al.(Wei et al., 2017) fabricated Sn-doped ZnO (ZTO) from a solution synthesized using a sol-gel process and used as an electron transport material in OSCs and found that the produced ZTO films had superior charge transport capabilities and smoother surface morphology after Sn alteration, especially when treated at a low temperature of 120 ^{o}C. Inverted OSCs with high-temperature (200 ^{o}C) treated ZTO films demonstrated the highest power conversion efficiency (PCE) of 9.32 %, which is higher than those with ZnO films processed at the same temperature (Wei et al., 2017). As already discussed in the above discussion, for OSCs, the energy level matching between the acceptor material and the ETL is critical for the efficient extraction of electrons, which greatly influences the device performance. The energy level diagrams taken from ultraviolet photoelectron spectroscopy (UPS) of ZnO and ZTO films used in this work are exhibited in Figure 7a which revealed that at the higher annealing temperature, the conduction band minimum (CBMs) of ZnO and ZTO are both around 4.0 eV, which matches well with the lowest unoccupied molecular orbital (LUMO) of PC71BM (Wei et al., 2017). However, at the lower annealing temperature, the CBM of ZnO dramatically increased to 4.3 eV while the CBM of ZTO maintained at the similar value. This energy level mismatch may lead to a larger electron extraction barrier at the interface and increase the exciton recombination rate in the active layer. From this finding it is possible to say that doping of Sn into ZnO structure (ZTO) can provide an improved ohmic contact between the ITO and the active layer. In addition to the band alignment, the ETLs' surface morphology has a significant impact on appropriate interface contact and electron transport through the interfaces. After adding the Sn, the prepared

ZTO films showed lower surface roughness (see Figure 7(b)), leading to the reduction in current leakage of devices Consequently, improved device performance because ZTO films with smoother surface can passivate the surface defects, decrease the contact resistance and enhance the flatness of active layers spin coated on them (H.-C. Chen et al., 2015).

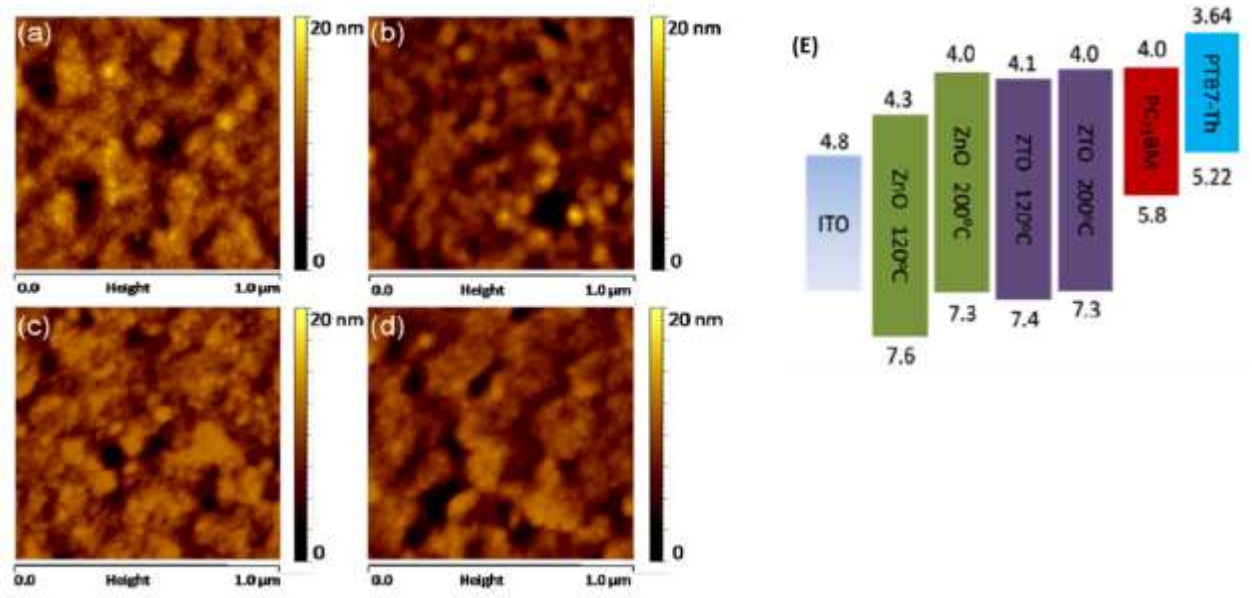

Figure 7. *AFM height images of ZnO and ZTO films (a) ZnO 120 ºC, (b) ZnO 200 ºC, (c) ZTO 120 ºC, (d) ZTO 200 ºC (a) UPS spectra of ZnO and ZTO films and (e) (Wei et al., 2017).*

However, rougher surface can also enhance the solar cells performance because it can provide higher contact area between the ETLs and the active layers. Regarding the several methods discovered to deposit a thin ZnO layer on substrates, there is no "elective" method to provide the optimum morphology; after all the deposition parameters have been tuned, each method can afford the best results (Lattante, 2014; X. Yu et al., 2013). According to Yu et al., (X. Yu et al., 2013) increasing the surface roughness of the ZnO layer boosted the power conversion efficiency of a P3HT:PCBM-based I_{SC} from 2.08 to 2.88 %. Because the surface roughness of the as-deposited (by sol-gel) ZnO layer is affected by three processes during annealing, such as solvent evaporation, zinc acetate decomposition, and crystallization, the surface roughness of the layer was changed by simply varying the annealing rate of the as-deposited (by sol-gel) ZnO layer, namely a slow annealing rate of 9 °C/min and fast annealing of 56 °C/min up to 300 °C. The increased light absorption due to the rougher ZnO surface, which should provide an efficient light trapping

mechanism is the reason for the increased J_{sc} because rougher surfaces scatter more light in multiple directions by the upper Ag electrode, lengthening the path length inside the active layer (Ohyama, Kouzuka, & Yoko, 1997).

Because FF is known to be highly connected to charge extraction efficiency at interfaces, the greater FF was explained by improved crystallization of ZnO due to the slow annealing rate, which resulted in more effective electron extraction and hole blocking (Z. Hu et al., 2011). Nickel, F., et al.,(Nickel et al., 2012) demonstrated that the annealing temperature is a key factor in determining the morphology of the layer: they annealed the ZnO films at three different temperatures, namely 130 °C, 150 °C, and 200 °C, and characterized them using photoluminescence and Raman measurements, found that the 150 °C annealed film was affected by better crystallization, which could enhance electron extraction and mobility, as well as suppress the leakage current. These findings suggest that in order to optimize both the crystalline structure and the surface roughness of sol-gel-derived ZnO films, both the annealing temperature and the annealing rate should be considered, with a trade-off between increased light scattering by the surface roughness (thus enhancing the active layer absorption, and thus the Jsc, and increasing the FF). Liang et al. reported a PCE of 3.3 % for the device with P3HT:PCBM active layer and based on a dense and homogeneous ZnO film driven from 0.1 sol due to an increase in the FF while J_{sc} only increases slightly and the V_{oc} remains almost unchanged (Liang et al., 2012). Moreover, Series resistance (R_S) was found to increase with increasing the surface roughness and the content of voids in ZnO film due to the reason that the dense ZnO CBL with a homogenous surface allowed the formation of intimate contact between the ZnO CBL and the BHJ photoactive layer, however a rough surface including voids led to inferior contact and an increase in the contact resistance (Liang et al., 2012). According to Ma et al., high surface roughness nano-ripple ZnO ETLs can contribute to high surface energy and a small donor/acceptor (D/A) interfacial area in the active layer put on top of ZnO CBLs, lowering the Jsc (Z. Ma et al., 2012). Furthermore, it has been suggested that the large surface area of ZnO CBLs may result in more trap-assisted recombination at the active layer/ZnO interface than smooth ZnO CBLs, lowering the FF of solar cells, resulting in the best-inverted PSCs with the smoothest ZnO layer, which gives the largest D/A interfacial area and the lowest ZnO/active layer interfacial area (Z. Ma et al., 2012). Yang et al.,(T. Yang et al., 2010) reported high-performance polymer solar cells (PSCs) with an inverted device structure using solution-processed ZnO thin film as a buffer layer, and obtained PCEs of 3.8% from PSCs with an inverted

device structure with ZnO as a buffer layer whereas, without the ZnO buffer layer, PSCs only show PCEs of 1.67%, which is less than half the value from PSCs with the ZnO buffer layer. Moreover, they also found that PSCs with the ZnO layer exhibited very good stabilities i.e. when operated at room temperature, there is no obvious degradation from the PSCs with the ZnO layer after continuously illuminating the devices for 4 h unlike PSCs without the ZnO buffer layer that undergoes significant degradation after illuminating the devices only for 1 h (T. Yang et al., 2010).

Low-temperature solution-processed ZnO CBLs' contribution to increasing the performance of inverted PSCs is limited because of the presence of high-density defects such as dangling bonds and surface groups, as well as the poor spatial distribution of nanoparticles over a large area (Cho et al., 2014). To obtain a good performance of inverted PSCs, homogenous ZnO NPs sheets with low-density defects must be developed.

Polymer-modified ZnO films, also known as ZnO/polymer hybrids or nanocomposites, have recently been investigated to tackle such issues (Small et al., 2012). Chen, H.-C., et al.,(H.-C. Chen et al., 2015) reported polyethyleneimine doped zinc oxide composites (ZnO:PEI) as efficient electron transport layers (ETL) for enhancing electron extraction in inverted polymer solar cells, demonstrated the power conversion efficiency (PCE) of the P3HT:PC61BM (1:1, w/w) device improved to 4.6 % when a composite of ZnO:PEI (93:7, w/w) was used as the ETL, up from 3.7 % when pure ZnO was used as the ETL whereas using the PBDTTBO:PC71BM device the PCE improved to 8.7% from 7.3 %. Figure 8 (a) shows the inverted BHJ system 1 or 2 device structure they tested i.e. as the electron donor, P3HT or PBDTTBO were used whereas as the electron acceptor, they used $PC_{61}BM$ or $PC_{71}BM$; BHJ systems 1 and 2 indicate P3HT:PC61BM and PBDTTBO:PC71BM, respectively.

The improvement in surface roughness of the ZnO layer and improved the structural order of ZnO in the ZnO: PEI layer which greatly boosted electron mobility in the vertical direction (see figure 6b) was the reason for the performance improvement (H.-C. Chen et al., 2015). Additionally, they investigated the passivation effect of PEI modification on surface defects of ZnO films by studying the photoluminescence (PL) spectra (see Figure 8 (c)) of ZnO:PEI films, which showed no apparent emission near 535 nm due to trap emission or surface recombination, indicating that very few oxygen vacancy defects and the PL peaked at 364 nm, indicating that very few oxygen vacancy

defects (Ye et al., 2005) . AFM surface topography images of ZnO:PEI composite layers comprising varying concentrations of PEI are shown in Figure 8d. The virgin ZnO surface, as well as those adding 1% and 9% PEI, had continuous rough and root-like structures (Figure 8d, (b, f)). The addition of PEI reduced surface roughness from 6.7 nm for pristine ZnO to 4.6 nm for a 7% PEI in the ZnO mix, potentially improving physical contact and creating strong molecular dipoles between the ITO electrode and the active layer, resulting in better PCEs.

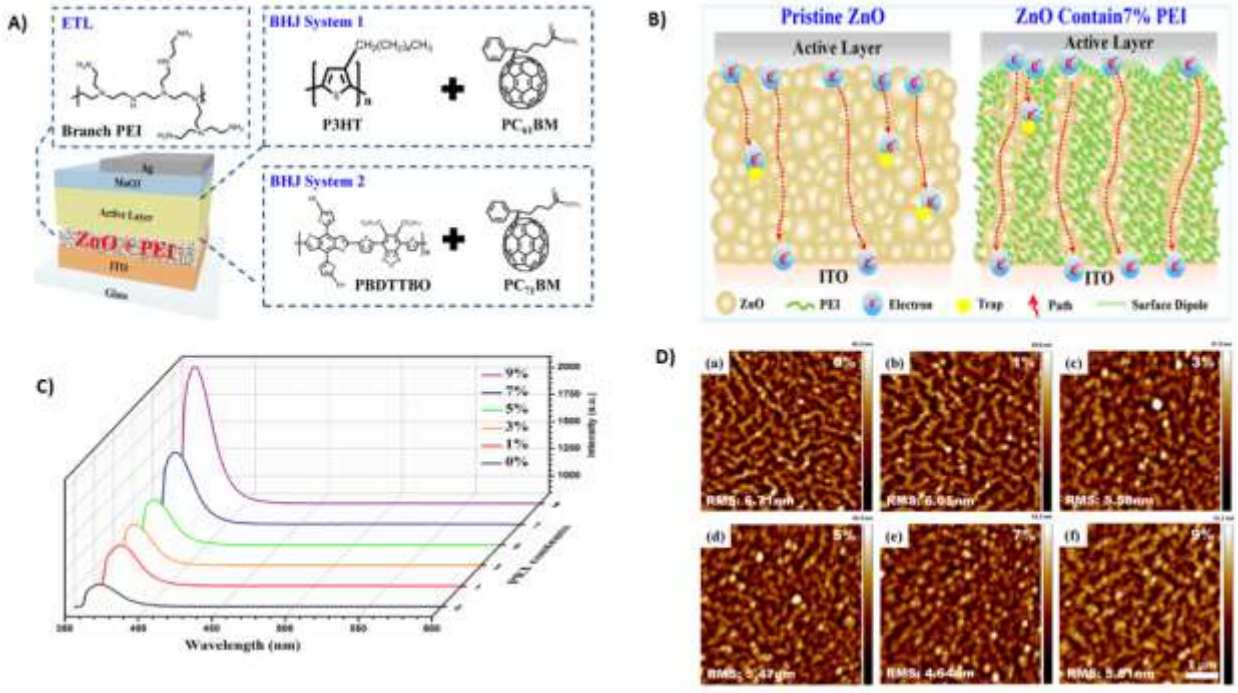

Figure 8. *(a) Chemical structures of the compounds used to prepare BHJ solar cells (b) structural order of ZnO in the ZnO:PEI thin films align perpendicular to the ITO electrode (C) PL spectra of ZnO:PEI nanocomposite films incorporating PEI at various contents (0%, 1%, 3%, 5%, 7%, 9%) (d) AFM topographic images of ZnO:PEI blends films incorporating PEI at contents of (a) 0, (b) 1, (c) 3, (d) 5, (e) 7, and (f) 9 wt. % (H.-C. Chen et al., 2015).*

Woo et al. (Woo et al., 2014) also reported an appreciable PCE enhancement in inverted PSCs by using an electron-rich polymer nano-layer (poly (ethyleneimine) (PEI)) modified ZnO CBL (Figure 9(a)), demonstrated that the enhanced PCEs is owning to the lowered conduction band energy of ZnO via the formation of an interfacial dipole layer at the interface between ZnO layer and PEI nano-layer (Figure 9 (b)). The recorded PCE of inverted PSCs of devices using only ZnO or PEI buffer layer show relatively low PCEs, 6.99% and 7.49%, respectively and the improvement

is attributed to the decreases in the series resistance of the device and the increase in surface roughness.

Bai et al.(Bai et al., 2015) established a facial ethanedithiol (EDT) treatment approach to passivate surface defects and alter intragap states of ZnO CBLs obtained with solution-processing at low temperatures with inverted structure (see Figure 9 (c)), demonstrated that covalent bonding of EDT molecules onto ZnO nanocrystals could remove various surface defects of ZnO nanocrystal layers by forming zinc ethanedithiolates during the EDT treatment, preventing chemical change through EDT-passivation, resulting in modulation of intragap states in pristine ZnO nanocrystals and the introduction of a new intragap band (see Figure 9 (e) and (f)).

Research effort on the methods of light absorption enhancement has been driven, including using photonic crystals, plasmonic enhancement, (J. M. Lee et al., 2015) and textures. In addition to the strategies outlined above, increasing the effective thickness of the photoactive layer while avoiding an increase in charge recombination in the scenario of a thick active layer is another way to improve the light harvest of the photoactive layer. Moreover, the usage of a vertically aligned one-dimensional (1 D) ZnO nanostructure in PSCs to create direct electron transport channels to promote charge carrier collection and transport has been examined to increase the effective thickness of the photoactive layer (Chou & Chen, 2014). Inverted PSC with ZnO nanorods (NRs)(see Figure 9 (g)) attract great attention because, after the charge separation at the polymer and fullerene interface, the photo-generated electrons at LUMO level of fullerene transfer to the conduction band of ZnO, the electrons quickly move to cathode electrode along the ZnO NRs, in view of high electron mobility of ZnO NRs ($\sim$15 cm^2 s^{-1} V^{-1} along c-axis) (Law, Greene, & Johnson, 2005) which is several orders of magnitude higher than what are typically found in most of the organic semiconducting materials. The average distance between the charge carrier generation sites and the surface of the ZnO electron collection layer would be shorter in devices with ZnO NRs than in solar cells without ZnO NRs, reducing charge recombination substantially and the SEM of vertical aligned 1 D ZnO nanowires is shown on Figure 7 (h). Small, C.E., et al.,(Small et al., 2012) reported a method for improving charge collection in inverted polymer BHJ solar cells using a ZnO–poly(vinyl pyrrolidone) (PVP) composite sol-gel film as the ETL and demonstrated inverted polymer solar cells that operate with PCEs more than 8% and certified efficiencies of 7.4%, the removal of PVP from the nanocomposite film by UV-ozone treatment leads to improved charge collection in inverted polymer solar cells due to better electronic coupling

between the ZnO nanoclusters within the nanocomposite film and PC71BM in the active layer. Ibrahem, M.A., et al.,(Ibrahem et al., 2013) Prepared thin layers of ZnO NPs using a simple method without utilizing any surfactants to stabilize the ZnO particles in solutions, simply dispersing ZnO powder in pure ethylene glycol followed by high energy ball milling at room temperature in a batch-type grinder and demonstrated that the ZnO particle size decreased with increasing grinding time down to an average particle diameter of 25 nm, obtaining final device PCEs over 3.5 % using ZnO NPs after grinding.

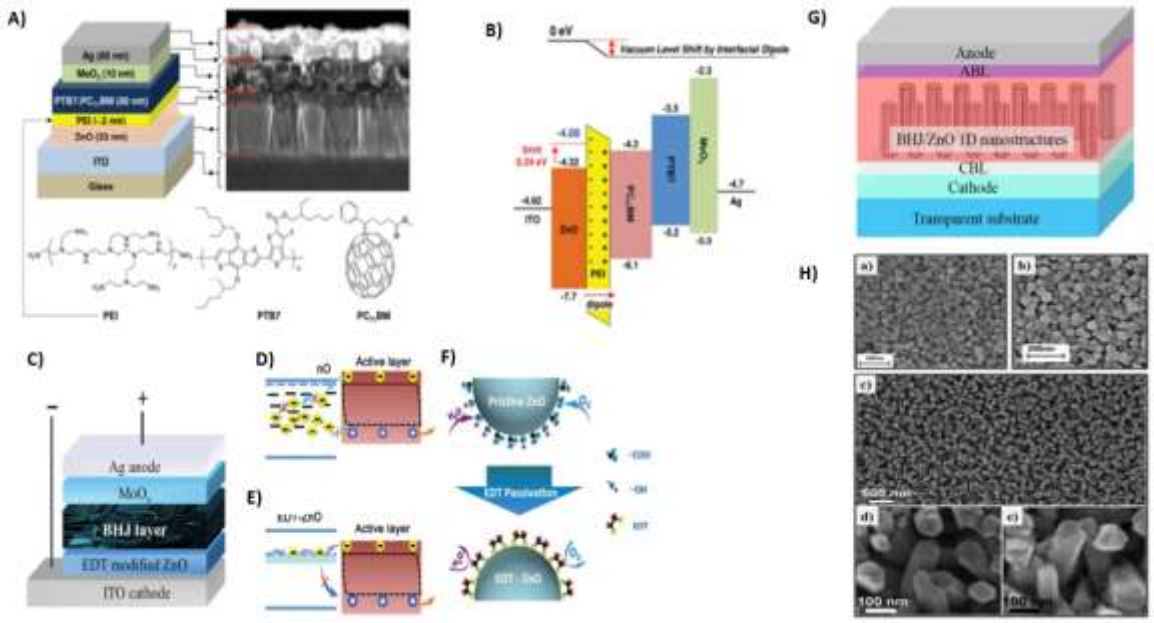

Figure 9*. (a) Schematic diagram of inverted PSC structure with 1 D ZnO nanorods. (b) Flat energy band diagram of the device with PEI-coated ZnO CBL. (c) Schematic illustration of inverted device structure with EDT modified ZnO CBL. (d) Various intragap states of pristine ZnO layers, which act as recombination centers for photogenerated charges. (e) The intragap states which facilitates electron transport in CBLs. (f) Schematic view showing that the various surface groups are removed and EDT molecules are covalently bound onto ZnO. (g) Top view of ZnO nanorods. (H)SEM images of 1 D ZnO nanostructures employed in inverted PSCs (Bai et al., 2015; Huang, Chou, & Lin, 2010; Woo et al., 2014).*

To sum up, although several attempts have been made to optimize the photovoltaic properties of P3HT:PCBM-based organic solar cells using ZnO ETLs doped with different metals, there is still

a large research space to use this material for PSCs using Sn doping. Furthermore, as discussed in the pieces of literature above, many studies have been reported by using ZnO ETL doped at fixed concentrations of dopants to modify the photovoltaic properties. Therefore, it is important to further explore the effect of dopants at different concentrations i.e. dopants such as Sn^{4+} so that the properties of the ETL would be improved. This in turn contributes to photovoltaics performance improvement. Presently, there have been no reported works using Sn^{-}doped ZnO ETL for P3HT:PCBM blend active layer based solar cell so, this study has contribution to understanding the effects of Sn at various concentrations on solar cell performance of P3HT based OSCs.

Table 1. Summary of the photovoltaic performance parameters for inverted Organic Solar Cells using ZnO electron transport layers. In the table, photovoltaic parameters values in parentheses represent those measured for a reference cell, while other parameters are defined earlier.

#	Device configuration	J_{sc} (mA/cm^2)	V_{oc} (V)	FF (%)	PCE (%)	Ref.
1	ITO/ZTO /PTB7Th:PC71BM/MoO_3/Al	17.51 (17.25)	0.8 (0.80)	66.71 (67.05)	9.32 (9.26)	(Wei et al., 2017)
2	ITO/ZnO:PEI/PBDTTBO:PC71BM/MoO_3/ Al	14.7 (10.3)	0.85 (0.60)	70 (60)	8.7 (3.7)	(H.-C. Chen et al., 2015)
3	ITO/ZnO / P3HT:PCBM/MoO_3/ Ag	10.39 (9.23)	0.53 (0.52)	46.2 (43.3)	2.55 (2.08)	(X. Yu et al., 2013)
4	ITO/ZnO/PSiF-DBT:PCBM/MoO_3/Au	5.03 (4.23)	0.9 (0.81)	60 (39)	3.8 (1.67)	(T. Yang et al., 2010)

5	ITO/AZO/PTB7:PC70BM/MoOx/Ag	17.1 (16.9)	0.74 (0.73)	70.6 (66.6)	8.86 (8.24)	(Jagadamma et al., 2015)
6	ITO/AZO/P3HT:PCBM/PEDOT:PSS/Ag	8.36 (8.41)	0.57 (0.57)	50.8 (53.9)	2.42 (2.56)	(Stubhan et al., 2011)
7	FTO/IZO/P3HT:PCBM/MoO_3/Ag	9.94 (8.39)	0.61 (0.61)	55 (57)	3.30 (2.94)	(Kyaw, Sun, Tan, Divayana, & Demir, 2010)
8	ITO/ZnO/P3HT:PsiF-DBT/MoO_3/Au	5.03 (4.23)	0.90 (0.81)	60 (39)	3.80 (1.67)	(T. Yang et al., 2010)
9	ITO/ZnO (SP)/P3HT:PCBM/WOx/Al	10.03 (8.91)	0.48 (0.41)	53 (50)	2.56 (1.76)	(Schumann et al., 2011)

10	ITO/ZnO/PCDTBT12:PC71BM/MoO_3/Al	9.78 (9.57)	0.98 (0.59)	57.7 (46.4)	5.53 (2.62)	(J.Sun et al., 2012)
11	ITO/ZnO/P3HT:PCBM/PEDOT:PSS/Ag	8.41 (6.86)	5.65 (4.26)	53.9 (29.2)	2.56 (0.85)	(Stubhan et al., 2011)
12	ITO/ZMO/PTB7:PC71BM/MoO_3/Ag	16.78 (14.64)	0.74 (0.75)	66.99 (64.75)	8.31 (7.11)	(Yin et al., 2014)
13	ITO/ZnO:Mg/P3HT:PCBM/MoO_3/Ag	9.7 (9.2)	0.58 (0.52)	56.8 (44.9)	3.17 (2.13)	(Tsai et al., 2013)
14	ITO/AZO/P3HT:PCBM/PEDOT:PSS/Ag	11.02 (10.73)	0.59 (0.58)	58.40 (53.73)	3.78 (3.32)	(Tsai et al., 2013)
15	ITO/ZnO/P3HT:ICBA/MoOx/Ag	10.79 (8.80)	0.83 (0.82)	60 (41.1)	5.39 (3.19)	(Brai, 2016)
16	ITO/ZnO-C_{60}/PTB7-Th:PC71BM/MoO_3/Ag	15.73 (14.02)	0.80 (0.79)	74.3 (69.1)	9.35 (7.64)	(S. H. Liao, Jhuo, Chen, &Ch, 2013)

17	ITO/ZnO-BisC_{60}/PTB7-Th:PC71BM/MoO_3/Ag	16.88 (15.32)	0.79 (0.79)	72.0 (67.1)	9.60 (8.12)	(S.-H. Liao et al., 2014)
18	ITO/ZnO/C_{60}-CAT/PCBM:P3HT/PEDOT:PSS/Ag	10.86	0.61	62.4	4.13	(Hau et al., 2010)
19	ITO/ZnO/C_{60}-PA/PCBM:P3HT/PEDOT:PSS/Ag	10.27	0.62	62.6	3.96	(Hau et al., 2010)
20	ITO/ZnO/C-PCBSD/ICBA:P3HT/PEDOT:PSS/Ag	12.4 (10.6)	0.84 (0.82)	60 (55)	6.22 (4.81)	(Stubhan et al., 2012)
21	ITO/ZnO-C60-EG/PTB7:PC71BM/MoO_3/Ag	15.86 (15.51)	0.73 (0.72)	69.1 (61.4)	8.0 (6.9)	(T. Hu, Chen, Yuan, &Chen,205)
22	ITO/ZnO-PAA/PBDTTPD:PC71BM/MoO_3/Ag	12.1 (11.9)	0.86 (0.84)	54 (46)	5.6 (4.6)	(Eita et al., 2015)
23	**ITO/ZnO:Sn/P3HT:PCBM/MoO_3/Al**	**10.69 (5.66)**	**0.61 (0.44)**	**53.01 (40.04)**	**3.45 (1.01)**	**this study**

CHAPTER THREE

3. EXPERIMENTAL METHODOLOGY

In this chapter, the materials used for the synthesis of Sn doped ZnO ETL, Photon absorber layer and the fabrication of solar devices are listed, general methods are introduced, and typical characterization techniques are included.

3.1 Materials and Chemicals

The chemical precursors and materials, that were used in this thesis are: Zinc acetate dihydrate ($Zn(CH_3CO_2)_2 \cdot 2H_2O$, Energy Chemical, 99.5%), Tin chloride dihydrate ($SnCl_2.2H_2O$, Loba,98 %), poly (3- hexylthiophene) (P3HT, Sigma-Aldrich), [6,6]-phenyl-C61-butyric acid methyl ester (PCBM, Sigma-Aldrich), 2-methoxyethanol($CH_3OCH_2CH_2OH$, Energy Chemical, 99%), Molybdnum Oxide (MoO_3, Sigma Aldrich) ethanolamine (CJ Chemicals, 99%) Chloroform (CF)(Chemical Co, 69%), Acetone (Dow Chemical, 99.5%), Ethanol (Loba Chemical, 99 %), Distilled water, ITO substrate, aluminum electrodes, micropipettes, aluminum foil, beakers, magnetic stirrer, drying oven, hot plate, thermal evaporator, UV-ozone cleaner and solar simulator in addition to the usual characterization instruments mentioned above. All chemicals are used without any further purification unless otherwise stated.

3.2 Methods

3.2.1 Preparation of Sn doped ZnO thin films

The pristine and Sn-doped ZnO films were prepared by adopting the procedure reported by Homnan, S., et (Homnan et al., 2021) with some modifications. Typically, a 0.52 M precursor solution was prepared by dissolving Zinc acetate dihydrate [$Zn(CH_3COO)_2 \cdot 2H_2O$] and Tin chloride dihydrate ($SnCl_2 \cdot 2H_2O$) in a mixture of 2-methoxyethanol (10 ml) and ethanolamine (as a stabilizer). The solution was stirred overnight vigorously at room temperature in air. The patterned ITO glass substrate was washed with soap and thoroughly cleaned using sequential ultrasonic treatments with, distilled water, acetone, and isopropanol for 20 min each. The cleaned ITO glass substrates were treated with UV-ozone cleaner for 20 min before depositing the ZnO films. Then the sol-gel processed pristine and Sn doped ZnO films were prepared by spin-coating the precursor solution twice onto the ITO substrates using a two-step spin coating process, at 1000

rpm for 10 s (first step) and at 2000 rpm for 30 s (second step). Then the films were annealed on the hot plate at 150 °C for 60 min in air, followed by cooling to room temperature before depositing the absorber layer.

3.2.2. Solar cell device fabrication

The electron transport layers were deposited via spin-coating, on cleaned glass substrates, from solutions of ZnO with or without the inclusion of Sn. Solar absorber films were then spin-coated on the dried ETL layers from the solution of an active layer composed of P3HT:PCBM blends at a 1:1 ratio. The active layer solution was prepared from P3HT and PCBM polymers by blending a stoichiometric ratio of 1:1, in chloroform solvent at a 20 mg/ml concentration, after stirring for 6 hours at 80 $^{\circ}$C. The prepared solution was spun at 500 rpm for 10 s followed by 1000 rpm for 30 s. Then the film was annealed on the hot plate in the air at 130 ^{0}C for 10 min, followed by cooling to room temperature. Finally to complete the device, a thin layer of MoO_3 as a hole transporting layer and Al as a hole collecting electrode were deposited continuously through thermal evaporation under a vacuum of ~5×10^{-6} Pa. The shadow mask was used during thermal evaporation to define the area of 0.04 cm^2. The schematic representation of the overall device fabrication process and device structure ITO/ZnO /P3HT:PCBM/ MoO_3/Al are shown in Figure 10.

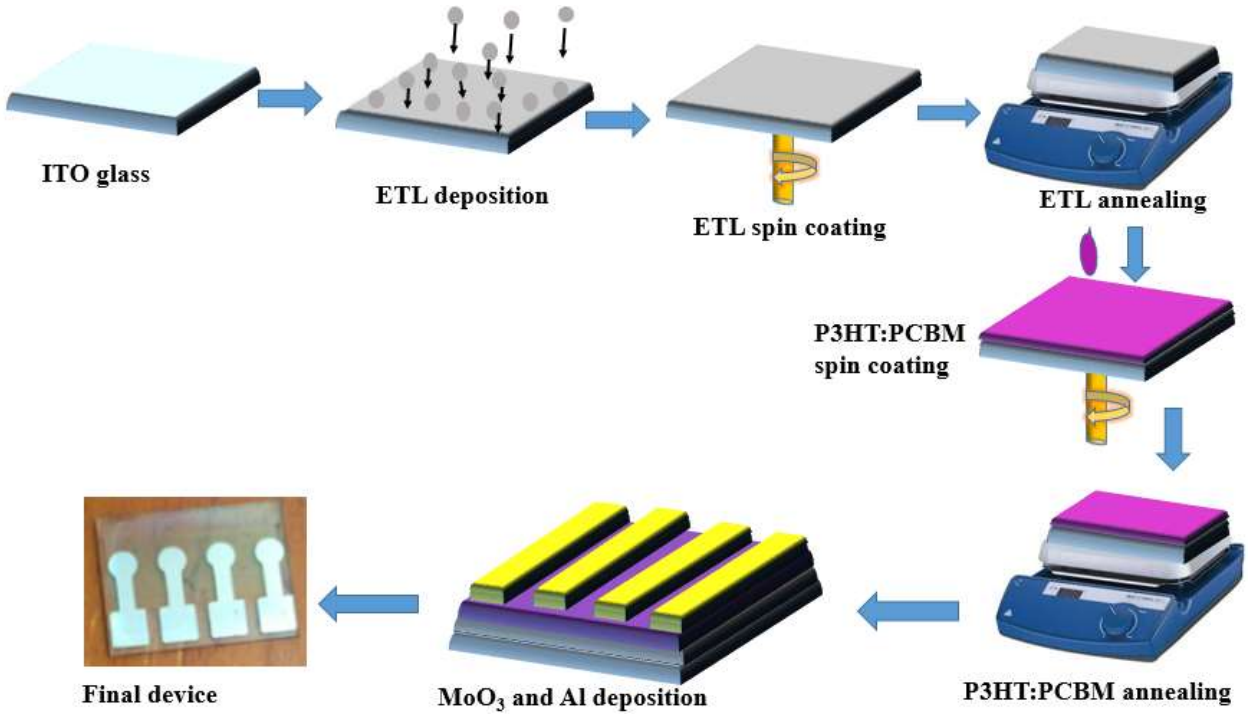

***Figure 10**. Schematic illustration of organic solar cells fabricated by one-step deposition method.*

3.3 Characterizations

3.3.1 Materials characterization and Photovoltaic performance measurements

Determination of crystal structure was carried out by using X-ray powder diffraction (Shimadzu XRD- 7000) at copper Kα radiation (λCuKa=1.5418 Å), the scan speed of 3.000 (deg/min), voltage (40 kV), current (30mA) and scanning range (10-80°). Absorption and photoluminescence (PL) spectra of the films prepared on glass were recorded using Perkin Elmer Lambda 19 UV-Vis/NIR spectrophotometer and HORIBA FLUROMAX- 4 spectrofluorometric, respectively. The optical absorption and transmission spectra were measured within the wavelength range of 250–1100 nm. The photoluminescence (PL) spectra of pristine and Sn-doped ZnO films were measured at room temperature at an excitation wavelength of 280 nm whereas the blend films and blend spin-coated on ZnO films were excited at 480 nm. The Raman spectra were performed using a Raman spectrometer (inVia Reflex, inVia-58P056), and the wavelength of the focused excitation laser was 532 nm (2.33 eV).

The electrical conductivity measurements of the ZnO layer with and without Sn dopant films prepared on the ITO substrate were carried out using two probe I-V measurement systems in dark to identify the effect of Sn on the charge conductivity of the electron transport layer (ETL). Photocurrent density–voltage (J-V) measurement was carried out under solar light operating at AM1.5 and integrated power intensity of 100 mW/cm^2 with computer-interfaced Keithley HP2400 source-meter and a solar simulator (model SS50AAA) to characterize the photovoltaic properties of the fabricated OSCs. Space charge limited currents (SCLC) for the active layer films made with pristine ZnO and ZnO doped with different concentrations of Sn were measured in electron-only devices with a configuration of ITO/ZnO:Sn/P3HT:PCBM/Al. The devices were prepared following the same procedure described in the Experimental Section for the photovoltaic devices. Figure 2 (a) and (b) illustrate the device structure and the energy band diagram, respectively.

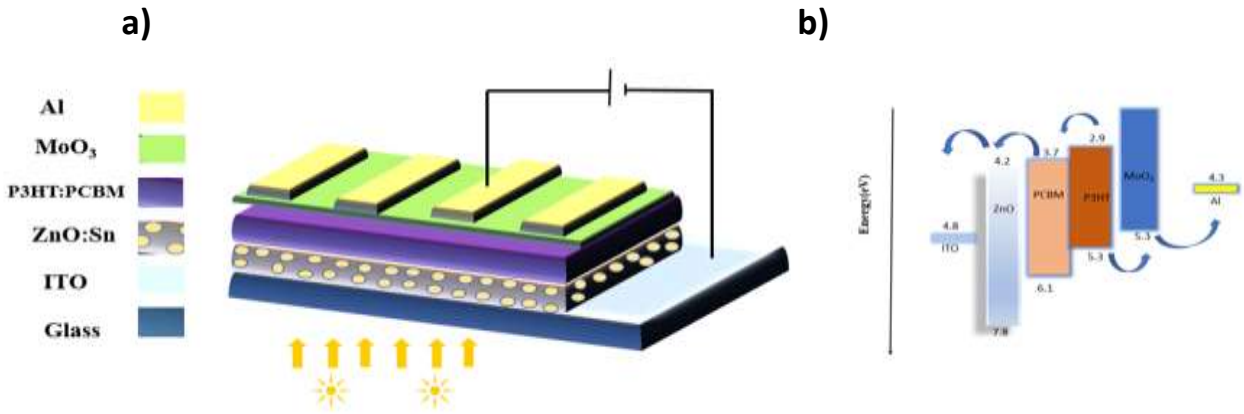

Figure 11. *(a) Schematic diagram (b) energy band diagram for device ITO/ZnO/P3HT:PCBM/MoO3/Al structure used in this study with pristine ZnO and ZnO doped with different concentration of Sn.*

CHAPTER FOUR

4. RESULTS AND DISCUSSION

4.1 XRD Analysis

Figure 12 illustrates the XRD spectrum of ZnO particles (a) and films (b) prepared without and with various Sn concentrations. The intense diffraction peaks for all ZnO particles were found at 31.81°, 34.45°, 36.29°, 47.59°, 56.67°, 62.93°, 66.53°, 68.01°, 69.27°, and 77.08°, which correspond to (100), (002), (101), (102), (110), (110), (103), (200), (112) and (201), respectively. The intense and well-defined diffraction peaks for all films correspond to (002) and (110) planes which much very well with card No. (JSPDF File No. 79-2205). All of the typical peaks for pristine and Sn-doped ZnO exhibited the hexagonal Wurtzite crystal structure, and no impurity was found, indicating that Sn was successfully incorporated into ZnO without affecting its crystal structure. It is clearly visible that planes (002) and (110) (see Figure 12b), are the preferred direction of crystal growth during the film annealing process which is consistent with the work reported earlier (Andolsi, Chaabouni, & Abaab, 2017; Ganesh, Yahia, AlFaify, & Shkir, 2017; M. Kumar et al., 2018; Rherari, Addou, Bougrine, El Jouad, & Haris). The broad peak observed at a diffraction angle of 24° corresponds to the glass substrate on which the film was deposited. In addition, as indicated by the inset plot, the (002) plane of all ZnO films and particles on the spectra showed a slight shift to the higher diffraction angle after Sn was introduced into the ZnO. This change is explained by the substitutional replacement of greater ionic radius Zn^{2+} (0.74 Å) with smaller ionic radius Sn^{4+} (0.69 Å), which agrees with (Ajili et al., 2013; Humayun, Kashif, & Hashim, 2013; Venkatesh et al., 2021). There is no distinguishable difference in the peak intensities of all ZnO films and nanoparticles diffraction after Sn doping and increasing doping concentration compared with the comparable peak in the ZnO. This suggests that Sn doping and increasing the amount of doping in the ZnO structure do not degrades its crystallinity, which could be attributed to the absence of stresses due to the small size difference between the Zn and the dopant ions, as well as dopant segregation at grain boundaries for high doping concentrations (Yousefi, Jamali-Sheini, Zak, & Mahmoudian, 2012).

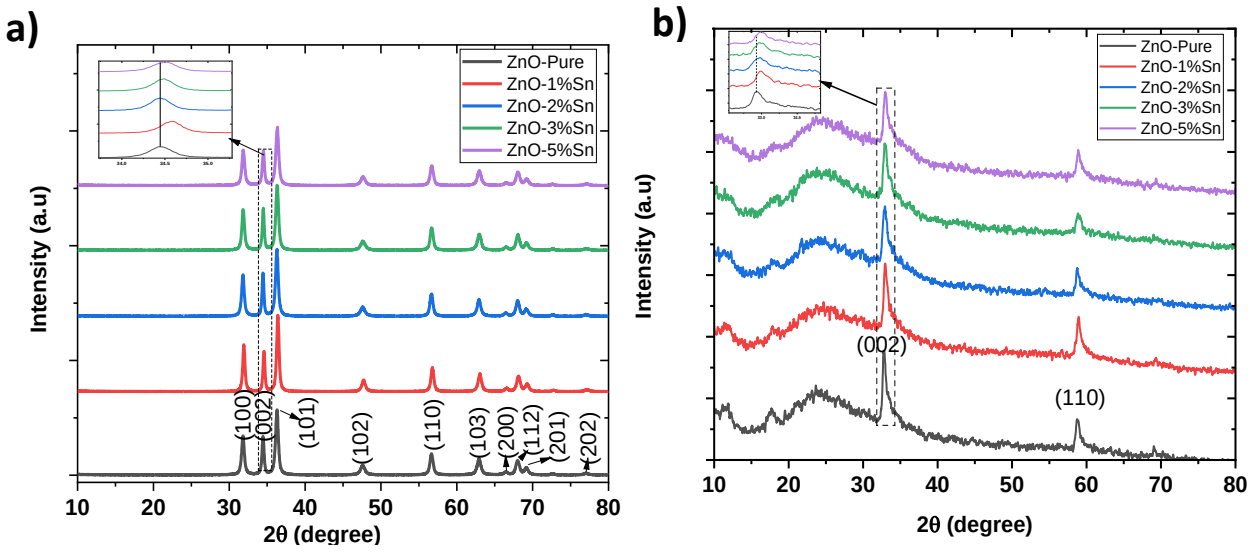

Figure 12. *XRD pattern of undoped and Sn-doped ZnO (a) particles and (b) films on glass.*

4.2 Optical properties of Sn doped ZnO ETL

The light transmittance, absorption, and PL spectra of the undoped and Sn-doped ZnO thin films prepared at different concentrations of Sn were investigated and shown in Figure 13. The transmission spectra of ZnO thin films on glass without and with Sn concentration at 1, 2, 3, and 5wt. % was measured and they are shown in Figure 13a. In an inverted BHJ solar cell, the transmittance of ETL is very important because the illuminated light must first pass through it before reaching the active layer. Therefore, high optical transmittance is beneficial to improve the utilization efficiency of solar radiation and will enhance the solar cell PCE (Qiu et al., 2017). Pristine ZnO film and ZnO films at all Sn loading concentrations had transmittance values of above 90 % in the visible range (400-800 nm) of the solar spectrum, indicating that this material is a good candidate for ETLs and allow a large fraction of light to be reach the P3HT:PCBM layer.

The bandgap of all films was calculated from their transmittance spectra (see inset in Figure 13a) using the Taulc plot $(\alpha hv)^2$ with respect to photon energy (eV), where h is Plank's constant, v is photon frequency, and α is absorption coefficient. Using the following equation, the absorption coefficient (α) of all ZnO thin films could well be determined from optical transmittance measurements using the calculation reported by Chen, H.-C., et al (H.-C. Chen et al., 2015) as:

$$\alpha = \frac{2.303}{d} \times \log\left(\frac{1}{T}\right) \qquad (3)$$

Where T and d represent the transmittance and the film thickness (60 nm), respectively. The optical bandgap energies for all films with Sn concentrations of 0, 1, 2, 3, and 5 % by weight were 3.57 eV, 3.15 eV, 3.16 eV, 3.18 eV, and 3.37 eV, respectively. The optical bandgap decreased at first with 1 wt. % Sn doping, then increased (blue-shifted) when the Sn content was increased to 5 % but still lower than the pristine ZnO film. The Burstein-Moss effect, also known as the band filling effect, is responsible for the blue shift i.e. the carrier concentration within the conduction band increases as the Sn doping concentration increases, pushing the Fermi level inside the conduction band to a higher energy level, resulting in bandgap widening (Nair, Nirmala, Rekha, & Anukaliani, 2011; Venkatesh et al., 2021). The decrease in the band gap after Sn doping compared to the pristine film is attributed to the formation of Sn related localized band tail state in the band gap (F. Z. Bedia et al., 2014), which agrees with the Sn doped ZnO films reported by Young Ran Park et al. (Yung, Liem, & Choy, 2009) i.e. the optical band gap reduction is due to the deep states in the bandgap.

The UV−Vis absorption spectra of ZnO films on glass without and with a various doping concentration of Sn is shown in Figure 13b. All the doped and undoped films show optical absorption spectra only in the ultraviolet (UV) region which is consistent with the transmission spectra. However, there is a shift in the peak position to the lower energy after doping which is beneficial for blocking the UV radiation from reaching the active layer hence illumination of UV light may induce degradation of organic active layers (F. Z. Bedia et al., 2014). Moreover, the absorbance shift towards the longer wavelength (lower energy) region is due to the doping of element Sn which forms additional energy levels acting as a shallow level inside the band gap (Bomila, Srinivasan, Venkatesan, Bharath, & Perinbam, 2018).

Figure 13c illustrates the Photoluminescence (PL) spectra of doped and undoped ZnO thin films excited by 298 nm at room temperature. Five emission peaks i.e. blue emission at 455, 465, and 493 nm, and green emission centered at 505 and 522 nm were observed. The emission peak observed at 455 nm is caused by the transition from Zinc interstitial to the valance band of the ZnO, whereas the emission peaks located at 465 and 493 nm arised due to defects caused by oxygen i.e. oxygen vacancy or oxygen interstitial (Bomila et al., 2018; A. S. Kumar, Huang, & Nagaraja, 2014). On the other hand, the green emission centered at 505 and 522 nm are caused by oxygen vacancy i.e. recombination of electrons of the singly ionized oxygen vacancy in the surface

of ZnO with photogenerated holes (Umar & Hahn, 2006; Qingzhi Wu et al., 2008). It can be seen that, compared to the undoped ZnO film, the intensity of all defect-related peaks decreased upon Sn doping which indicates charge carrier recombination was suppressed as a result of a reduction in the defects which were active as a center for recombination. The ZnO film with 3wt. % Sn exhibited the lowest PL intensity compared with ZnO films with other concentrations, revealing better inhibition recombination at this Sn concentration which is beneficial for better charge carrier mobility in the ZnO electron transport layer wh ized in photovoltaic application.

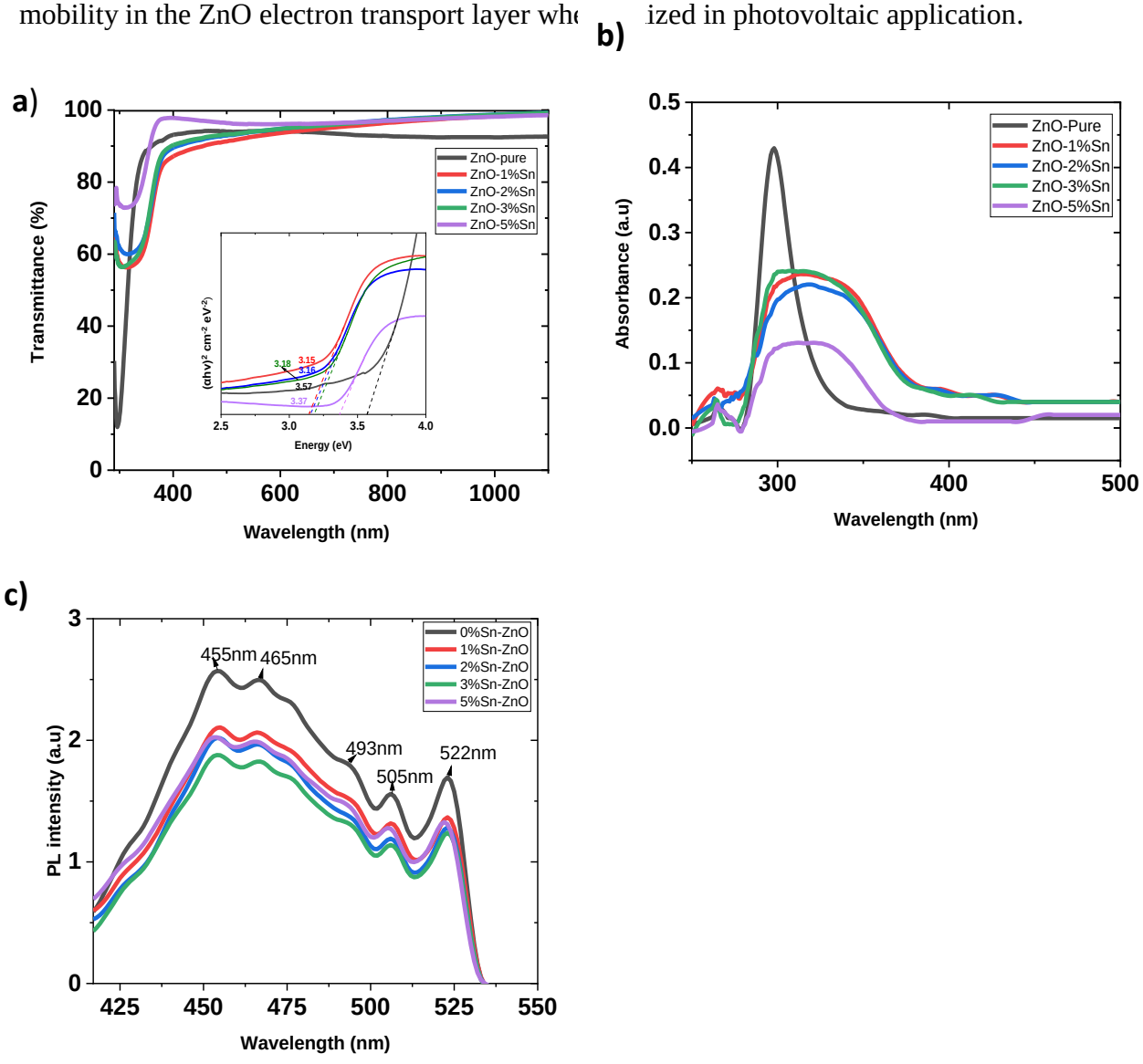

Figure 13. *(a) transmission (inset is tauc plots), (b) absorption and (c) PL spectra of thin films with structure glass/ZnO with pristine ZnO and ZnO doped with different concentration of Sn.*

4.3 Electrical properties of Sn doped ZnO ETL

For further investigation of the electrical properties of ZnO thin films with different Sn-doped concentrations, the current-voltage (I-V) characteristic curves of ZnO films with a device structure of ITO/ZnO:Sn/Al (inset in Figure 14a) were recorded in dark conditions, and the I-V curves of all devices are plotted in Figure 14a. The conductivity of Sn doped and undoped ZnO devices was calculated from the slope of the I-V curve using the formula reported earlier (Bomila et al., 2018; Choi et al., 2018):

$$\boldsymbol{\sigma = G \times L/A} \qquad (\mathbf{4})$$

Where σ is the electrical conductivity, G is the conductance (slope on the I-V curve), L is the thickness of the film (120 nm) and A is the active area ($0.04cm^2$).

Figure 14b presents the obtained electrical conductivity plot against the dopant concentration and the values of conductivity were summarized in Table 1. As indicated in Figure 14a, the undoped device exhibited less ohmic behavior and conductivity whereas the ohmic and conductivity behavior of the Sn-doped device were significantly improved. The increase in the electrical conductivity can be caused by the oxidation of Sn dopant to Sn^{4+} due to its easy oxidation property, so that it substitutes Zn^{2+} ion in ZnO crystal structure, impairing two more free electrons which contribute to the higher electronic conduction as reported earlier (Ajili et al., 2013; YC Lin, Hsu, Hung, Chang, & Wen, 2012). More Sn dopant ions can reside in the lattice site of Zinc with increasing Sn concentration as long as enough Zinc site is available for occupancy, increasing the electrical conductivity.

Figures 14 (a) and (b) indicate that the highest electrical conductivity of about 7 $x10^{-5}$ S/m of the ITO/ZnO:Sn/Al device was obtained at Sn concentration of 5wt. %. The ZnO films incorporated with 3 % and 5 % Sn by weight doping concentration exhibited almost twice higher conductivity compared with pristine film and in turn, this is responsible for lowering in series resistance of OSCs device and better electron transport from the absorber layer to the ITO which are beneficial for photovoltaics performance improvement. For instance, the existence of non-ohmic contacts between the electrode and the organic layers may result in a reduced V_{oc}, whereas the use of interfacial layers for better electron transportability improved J_{sc}.(J.-Y. Lee, Kim, Song, & Moon, 2011; Xin et al., 2012).

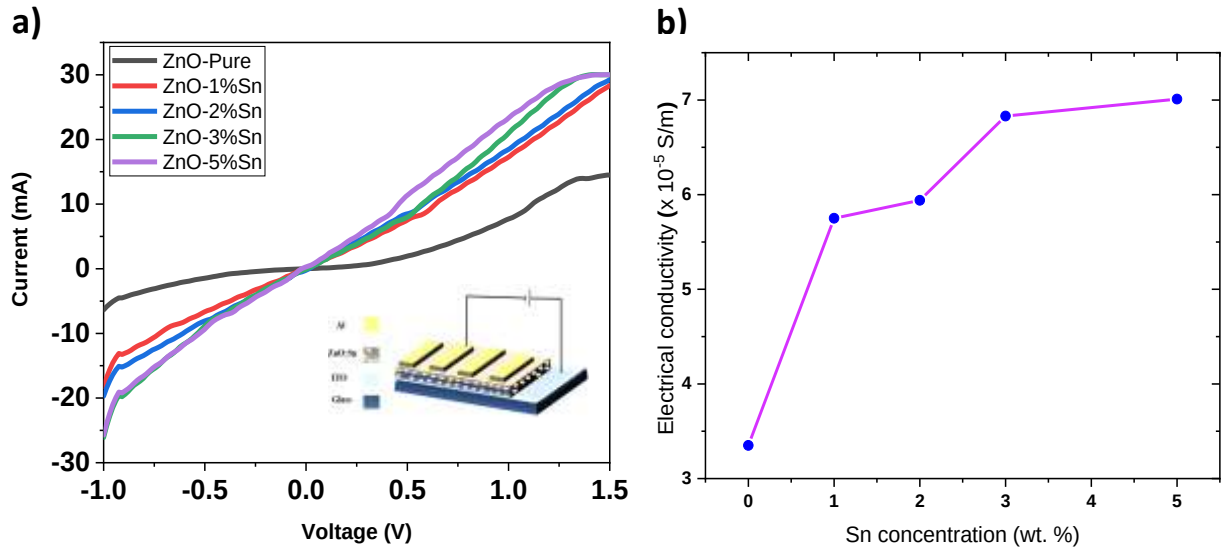

Figure 14. *Plot showing the I-V curve (a) and calculated electrical conductivity of thin films with structure ITO/ZnO/Al with pristine ZnO and ZnO doped with different concentrations of Sn* (b).

Table 2. Electrical conductivity of ITO/ETLs/Al films with different concentrations of Sn

Sn conc. (wt. %)	Conductivity (S/m) x 10^{-5}
0	3.35
1	5.75
2	5.94
3	6.83
5	7.01

4.4 Raman analysis

Figure 15 presents the Raman analysis of pristine and Sn-doped ZnO films with maximum photovoltaic performance. This analysis is performed to determine the structural components in the prepared ZnO films. There are two phonon modes in the bulk ZnO namely, longitudinal optical (LO) and transverse optical (TO) which are further split into A_1 and E_1 symmetries(Singh, Kumar, & Singh, 2020). Two non-polar Raman active phonons with E_2 symmetries also there with low

and high-frequency E_2 modes correspond to the vibration of Zinc ion lattice and oxygen ion lattice respectively(Singh, Singh, & Kumar, 2021). The peak observed at 440 cm^{-1} corresponds to the E_2 (high) mode of non-polar optical phonons which is assigned to the characteristic peak of the hexagonal wurtzite phase and the vibration of oxygen ion lattice suggesting the wurtzite ZnO structure was not destroyed by Sn incorporation (A. S. Kumar et al., 2014; Singh et al., 2021). The Rama peak at 560 cm^{-1} is assigned to the E_1 (LO) mode and this peak is exclusively present only in Sn-doped ZnO films which is weak for 3 % but strengthened when the sample is doped at 5 % of Sn by weight. The ion incorporation process introduced defects and impurities within the ZnO crystal, disrupting its translational symmetry and causing disorder-activated Raman scattering (DARS)(M. Wang et al., 2015). Peaks at 780 cm^{-1} and 1080 cm^{-1} are attributed to $2A_1$ (TO) second-order polar mode and multipolar mode, respectively, with intensity increasing as Sn concentration increases. Additionally, the intensity of these modes are strongly improved in Sn-doped ZnO films which is significant for 5 % Sn-doped film, the enhancement in the intensity of Raman peaks may also be attributed to the modified crystallinity of the films because of the doping(Samavati et al., 2017). Furthermore, the doped films appeared to have a peak at 2420 cm^{-1}, which is more evident at 5wt % Sn. This result demonstrates that the Sn ion has been readily incorporated into the ZnO system.

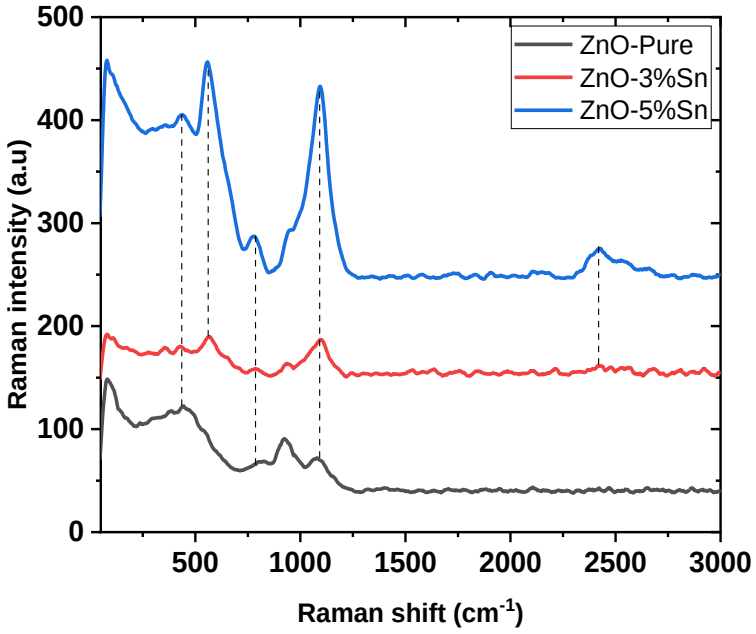

Figure 15*. Raman spectra of undoped and Sn doped ZnO films.*

4.6 Optical properties of OSC films

To understand the effect of different Sn concentrations on the optical properties of spin-coated ZnO ETL and ZnO ETL with different concentrations of Sn, the light absorption and PL spectra of glass/ZnO:Sn/P3HT: PCBM devices were investigated, and shown in Figure 15 (a) and (b), respectively. Note here that the active layers of all the films were prepared from the same solution and spin-coated at the same speed to keep their thickness similar which allows direct comparison of optical properties. The active layer with ZnO ETL doped at 3 wt. % Sn exhibited the highest absorption peak intensity (Figure 16a). The highest absorption peak could be related to the higher surface roughness, which may have a larger contact area with the active layer which is useful to trap and scatter the incoming light into the active layer (Ikram, Murray, Imran, Ali, & Shah, 2016; H. Peng, Xu, Zhou, Zhang, & Li, 2015). Moreover, the UV–vis spectra do not show any ZnO-related absorption peak suggesting that the ZnO layer were transparent as shown in Figure 13. The enhanced optical absorption in Sn doped-based samples can result in an enhancement in the generation of exciton and thus improves the J_{sc} and overall device performance (Thaver, Oseni, & Mola, 2021).

Figure 16b depicts the PL spectra of P3HT and P3HT:PCBM coated on doped and undoped ZnO ETL films recorded at room temperature at an excitation wavelength of 488 nm. The PL intensity of P3HT-only film was significantly higher because of maximum exciton recombination due to the absence of an exciton dissociation pathway. However, the PL of P3HT was quenched when blended with PCBM due to exciton dissociation at the donor/acceptor interface. Following the exciton dissociation, the electron in the PCBM will be transferred to the ETL further reducing the chance of recombination thus reducing the PL intensity as shown in Figure 16b. An efficient electron transfer is beneficial for solar cell application The exciton quenching efficiency (QE) in the films were calculated using equation 5 (Tegegne, 2018) and is summarized in Table 3. The PL quenching efficiency (QE) is calculated as:

$$\boldsymbol{QE}\ (\%) = \frac{\mathbf{PL_{blend}}}{\mathbf{PL_{polymer}}}\mathbf{X100} \qquad (\mathbf{5})$$

, where PL_{blend} and $PL_{polymer}$ correspond to the PL recorded in the P3HT:PCBM/ELT/Glass and the P3HT/Glass, respectively.

The PL quenching efficiency appeared to increase with increasing Sn concentration in the ZnO layer, reaching its maximum value (80.5 %) at 3 wt. %. This is the key indicator of successful exciton dissociation at the D/A interface and effective charge extraction from in the P3HT-based solar cell (J. Wang et al., 2013).

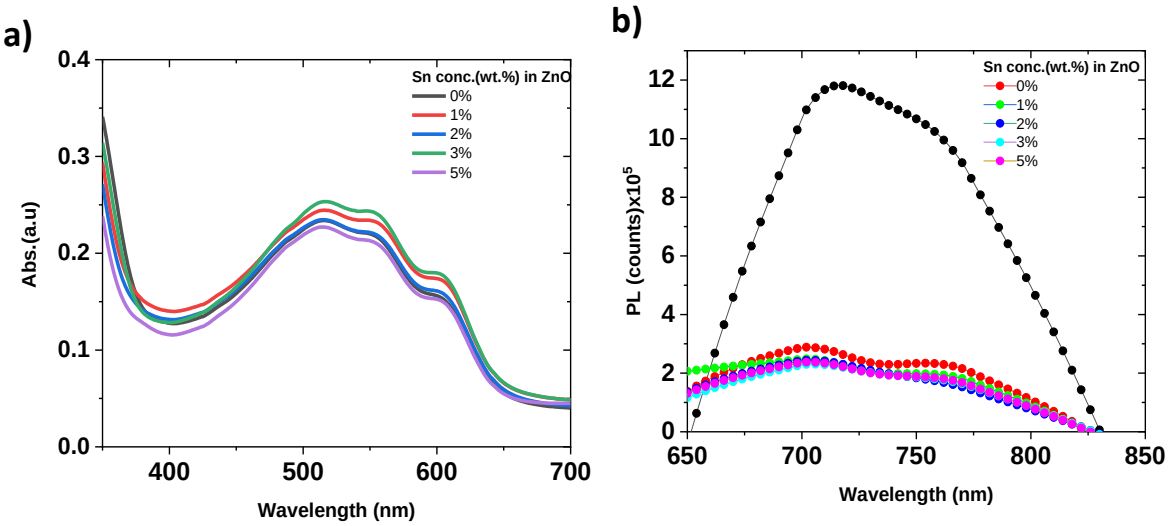

Figure 16*. Plot showing absorbance (a) and PL spectra of the film with structure Glass/ZnO/P3HT: PCBM (b) with pristine ZnO and ZnO doped with different concentrations of Sn.*

3.6 Photovoltaic properties

The bulk heterojunction organic solar cells were fabricated in an inverted structure with a different layer of materials as shown in Figure 11. The current density-voltage (J-V) characteristics of the fabricated device under the illumination of AM 1.5 solar simulator operating at a light intensity of 100 mW/cm^2 and in the dark are given in Figure 17 (a) and (b), respectively. The corresponding solar cell parameters such as the open-circuit voltage (V_{oc}), short-circuit current densities (J_{sc}), fill factor (FF), power conversion efficiency (PCE), series (R_s), and shunt (R_{sh}) resistances are summarized in Table 3. The P3HT: PCBM active layer with pure ZnO as ETL exhibited V_{oc}, J_{sc}, FF and PCE of 0.44 V, 5.66 mA/cm^2, 40.04 %, and 1.01 %, respectively. The device with ZnO ETL doped at 1 wt% Sn showed V_{oc}, J_{sc}, FF, and PCE of 0.52 V, 6.71 mA/cm^2, 43.83 %, and 1.53 % respectively. The 2 wt. % Sn doped ZnO ETL device exhibited V_{oc}, J_{sc}, FF and PCE of 0.6 V, 8.95 mA/cm^2, 46.43 % and 2.48 %, respectively. The efficiency of the inverted organic solar cell fabricated with 3 wt. % Sn-doped ZnO exhibited the best photovoltaic performance among all the devices, with PCE of 3.45 %, J_{sc} of 10.69 mA cm^{-2}, V_{oc} of 0.61 V, and FF of 53.01 %. The device

with ETL of 5 wt. % Sn doping exhibited V_{oc} of 0.62 and J_{sc} of 11.54 mA/cm^2 whereas the corresponding FF and PCE were decreased to 45.36 % and 3.25 % respectively compared to devices with ZnO doped at 3 wt. %. A substantial improvement in the PCE is derived from the inclusion of the Sn in the ZnO layer which is advantageous to optimizing charge dissociations, charge mobility, and collection processes (Hamed, Ike, & Mola, 2021), and this improvement originates from the enhanced V_{oc}, J_{sc}, and FF (Table 3). The device performance was highly improved with a gradual increase of Sn concentration up to 3 wt. % (see figure 17 (c)). This increase in the performance exhibited 340 % growth in efficiency from 1.01 % (undoped device). However, the efficiency dropped by 6 % when Sn concentration increased from 3 % to 5 % by weight. This is evidenced by the existence of higher R_s and lower R_{sh} which could be related to the difficulty in the flow of free charge carrier after dissociation in 5 wt. % based device. Moreover, the R_s value of all the Sn-doped ZnO-based devices are significantly lower and R_{sh} is significantly higher than the pristine ZnO-based devices resulting in increased PCE values. The FF is a measure of recombination and it depends on the photogenerated carriers extracted out of the device and is also strongly related with a series resistance of the device (R_s) (Bartesaghi et al., 2015; Tegegne, 2018). This lowest R_s resulted in the reduced recombination (increase in FF) in a 3 % doped ZnO device (Dlamini, Mbuyise, & Mola, 2022). The enhanced value of FF in the device treated with ZnO doped at 3 wt. % compensate for the lower value of J_{sc}, leading to the best PCE of 3.45 %. The charge transport process from the active layer to the respective transport layers significantly affects the J_{sc} output from the device hence the dissociated carriers within the blend copolymer prefer an uninterrupted and continuous pathway to reach their respective electrodes (Tegegne, 2018; Thaver et al., 2021). Therefore, the lower J_{sc} at 3 wt. % doping concentration compared to ZnO with 5 wt. % is attributed to its lower electrical conductivity as indicated on figure 14.

The V_{oc} of the device is the main indicator of the energetics of the layers and interfaces. The solar cell device with undoped ZnO ETL exhibited the lower V_{oc} compared with the device with ZnO ETL doped with Sn at different concentrations. This can be due to the lowered LUMO mismatch between the active layer and ZnO which reduces the barrier for electrons to be transferred from the active layer to the ETL. This is consistent with the calculated QE (see Table 4). As discussed in section 4.3, the Sn dopant increases in the electrical conductivity of the device due to a reduction in the trap states in the ETL layer, which is consistent with the PL and I-V measurement of ETL discussed above (Amollo, Mola, & Nyamori, 2020). However, the devices with the ETL at

concentrations of 2, 3, and 5 wt. % Sn exhibited comparable performance in terms of V_{oc}. This indicates the active layer/ETL energy band alignment has changed slightly at these concentrations and good ohmic contact between the ETL and the photoactive layer is already established at 2 % concentration (Dlamini et al., 2022). Figure 17 (b) depicts the current density-voltage (J-V) curves recorded under dark conditions for the devices with ZnO as ETL incorporated at different concentrations of Sn. As indicated, the device with Sn-doped ETL showed lower leakage current and higher forward bias current. We note that the 3 wt.% Sn doped ZnO device cell exhibits a slightly lower leakage current in the forward voltage regime, corresponding to a higher shunt resistance (R_{sh}) of 7507 Ω cm^2 with respect to that of 6681 Ω cm^2 for 5 wt.% Sn doped ZnO device (Table 3). This is consistent with the relatively high fill factor of the former solar cell.

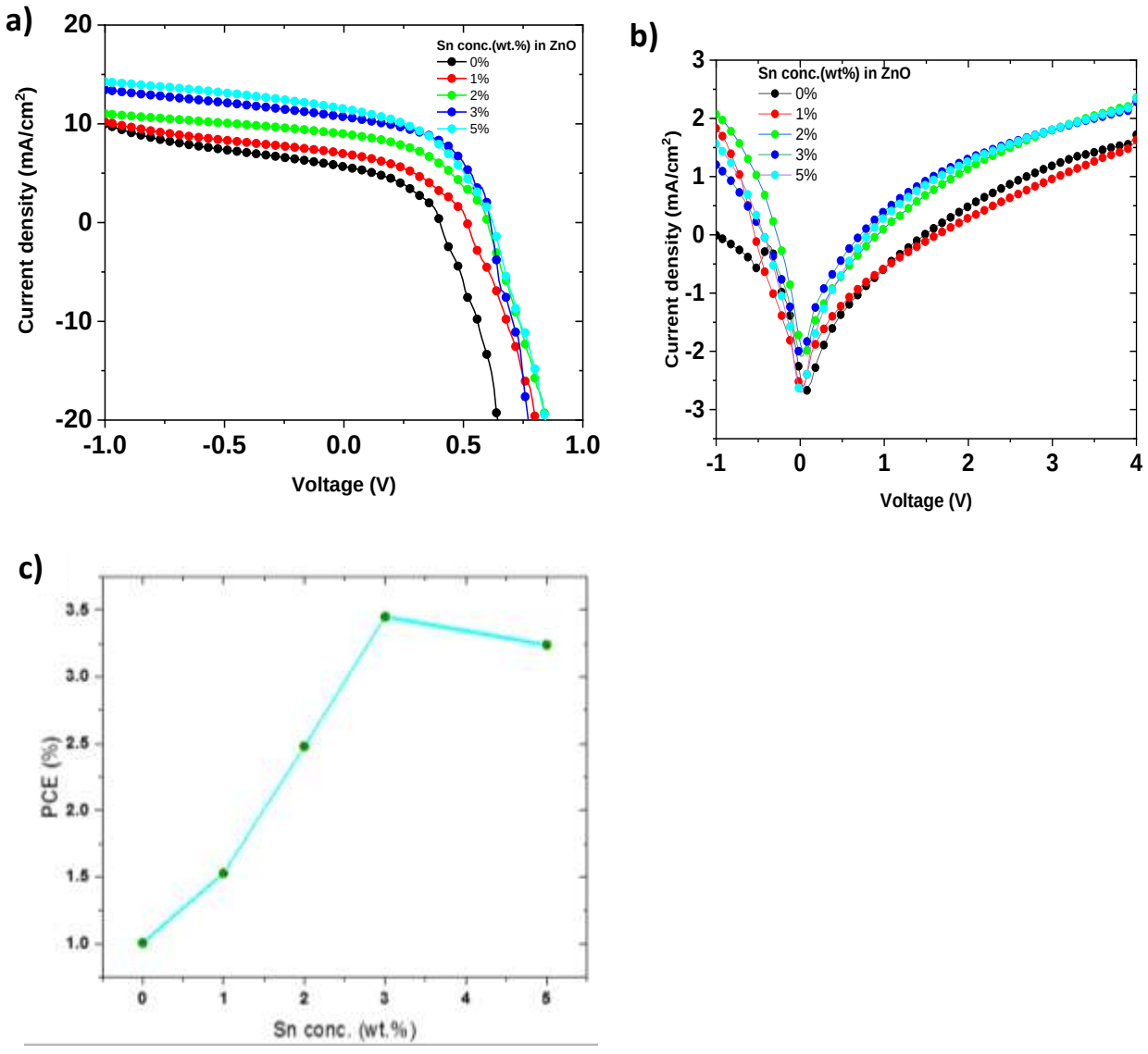

Figure 17*. J-V characteristics of solar cells with structure ITO/ZnO/P3HT:PCBM/MoO_3/Al where ZnO is incorporated with different Sn concentration under AM 1.5G illumination at 100 $mWcm^2$ (a), under dark (b), PCE versus Sn concentration (c)*

Table 3. Summary of device performance for solar cell structure with ITO/ZnO (with different concentrations of Sn)/P3HT:PCBM/MoO_3/Al

Sn conc. (wt. %)	V_{oc}	J_{sc}	FF (%)	PCE (%)	R_s ($\Omega.cm^2$)	R_{sh} ($\Omega.cm^2$)
0	0.44	5.66	40.04	1.01[a] (0.92)[b]	688	1949
1	0.52	6.71	43.83	1.53[a] (1.38)[b]	495.3	9468
2	0.60	8.95	46.43	2.48[a] (2.12)[b]	381.6	8785
3	0.61	10.69	53.01	3.45[a] (3.33)[b]	316.6	7507
5	0.62	11.54	45.36	3.24[a] (3.07)[b]	370.2	6681

[a] The maximum PCE [b] average PCE of 4 devices

4.7 Study of charge generation and exciton dissociation

The current that is recorded under illumination is the sum of the current under dark (J_D) and photogenerated current (J_{ph}). At open-circuit voltage, the illumination current is zero and, hence, the dark current is canceled by the illumination current. We can analyze charge generation and transport loss by examining photocurrent density (J_{ph}) as a function of effective voltage (V_{eff}), which has a significant link with the J_{sc} and FF (Qiang Wu et al., 2020). For example, if J_{ph} currents for the solar cells cannot be saturated, showing that J_{ph} is field-dependent which is related to significant recombination in the solar cell devices, resulting in a low FF (Zhen Wang et al., 2019).

Figure 18 shows the photon-dependent current density (J_{ph}) versus effective voltage (V_{eff}) curves of the fabricated OSC integrated with ETL with different Sn concentrations, and the corresponding results were summarized in Table 4.

The current density created by photons, $J_{ph}= J_L - J_D$ (where J_L and J_D represent the current density under illumination and in the dark, respectively), and the dependence on the effective applied voltage, $V_{eff} =V_0 - V_a$ (where V_a is the applied voltage, and V_0 is the voltage at which $J_L =J_D$)(Kim, Ahn, Wang, & Park, 2015), are plotted. As shown in Figure 18, two separate regions were

observed: i) the region in which J_{ph} rises linearly with applied voltage, where the influence of charge extraction prevails; and ii) the region in which the dependency departs from linear rather than saturates at high voltages, where the influence of charge generation dominates (Cowan, Roy, & Heeger, 2010). J_{ph} is saturated for OSC made from ZnO as ETL with and without incorporation of Sn at a high voltage (V_{eff} > 0.5 V), indicating that the photogenerated excitons are dissociated by the electric field into free charge carriers, which are swept out and collected by the electrodes (K. Wang et al., 2015). If J_{ph} is independent of temperature and applied voltage, the saturation current densities (J_{sat}) are only dependent upon the amount of absorbed incident photon flux being absorbed by the active layer. However, the V_{eff} where J_{ph} saturated is not the same i.e. the devices with ETL doped at 3 and 5 wt.% saturated at lower V_{eff} compared to device with pristine ZnO, suggesting that greater charges were generated and efficient charge transport in former devices compared with the later one(Kim et al., 2015). A higher J_{ph}-V_{eff} characteristic of the optimum device (3 wt. % Sn) proves the lowering of bimolecular recombination (evidenced by its high FF) and the free charges were swept out more efficiently at lower $V_{eff.}$ We recommend the readers to further study the intensity dependence of J_{ph} to further investigate bimolecular recombination phenomena.

Since the more efficient carrier transport directly causes an increase in J_{sat}, we calculated the maximum exciton generation rate (G_{max}) by using the formula $J_{sat} = qLG_{max}$ where q and L represent the electronic charge and the active layer thickness (120 nm) respectively. As summarized in table 3, the G_{max} values for the pristine ZnO and Sn incorporated ZnO were 4.24×10^{21} $s^{-1}cm^{-3}$, 4.61×10^{21} $s^{-1}cm^{-3}$, 5.36×10^{21} $s^{-1}cm^{-3}$, 8.03×10^{21} $s^{-1}cm^{-3}$and 7.15×10^{21} $s^{-1}cm^{-3}$, respectively and we might say from these findings that adding 3 % Sn to the device's ZnO ETL enhanced G_{max} considerably.

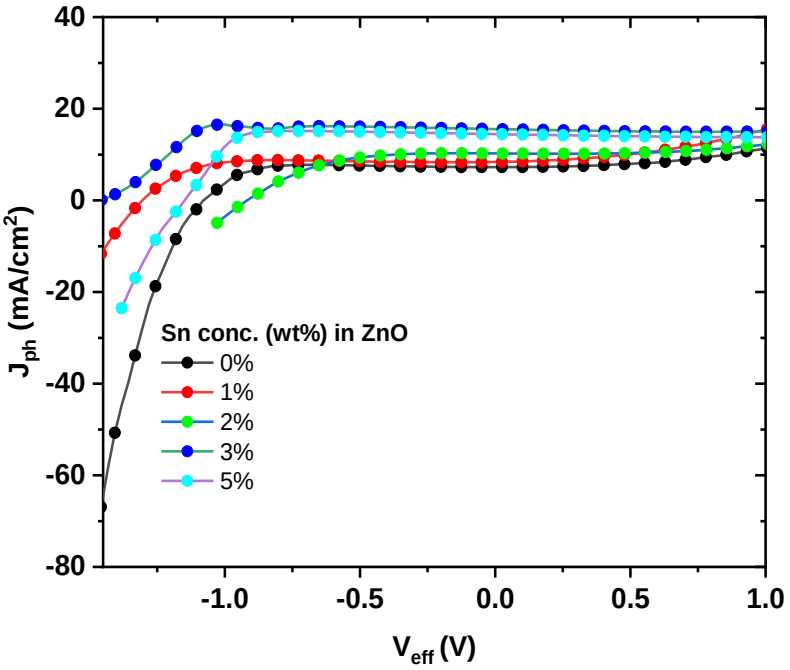

Figure 18. *The Jph (JL – JD) vs Veff (V0 – Va) characteristics of OSC with pristine ZnO and ZnO incorporated with different concentration of Sn.*

Table 4. QE. Jsat and Gmax of OSC under short-circuit condition with various concentration of Sn

Sn conc. (wt. %)	QE (%)	J_{sat} (mA/cm^2)	G_{max} ($s^{-1}cm^{-3}$)x10^{21}
0	77	8.15	4.24
1	78.5	8.86	4.61
2	78.8	10.32	5.36
3	80.5	15.45	8.03
5	79.2	13.75	7.15

4.8 Study of charge mobility

To suppress the photogenerated current in the devices, space charge currents are monitored in the dark so that carriers emerge from the electrodes by injection through the external circuit. To study the electron mobility of the device with ZnO ETL at different concentrations of Sn, the electron-only device was fabricated (Figure 19) and the corresponding electron mobility was calculated through space limited current (SCLC) model using the Motto-Gurney SCLC equation reported elsewhere(Dlamini et al., 2022; Hamed et al., 2021) as:

$$J_{SCLC} = \frac{9}{8}\mu_e \varepsilon_o \varepsilon_r \frac{V^2}{L^3} \quad (6)$$

Where, μ_e, ε_o, ε_r, V and L the electron mobility, vacuum dielectric constant (ε_o=8.95x10^{-12} F/m), the dielectric constant of P3HT: PCBM (ε_r=3) (Han et al., 2014), the applied voltage and the thickness of the absorber layer (120 nm), respectively. Where the applied electric field causes the charge to change, μ_e is then given by the expression:

$$\mu_e = \mu_0 \exp(\gamma\sqrt{E}) \quad (7)$$

Where μ_o is the zero-field mobility, **γ** is the field-dependence activation factor and $E = V/L$ is the applied electric field. Applying this equation and rearrangement, equation (6) becomes:

$$J_{SCLC} = \frac{9}{8}\mu_e \varepsilon_o \varepsilon_r \exp\left(0.89\sqrt{\frac{V}{L}}\right)\left(\frac{V^2}{L^3}\right) \quad (8)$$

From the fit (Figure 20) using equation (8), the extracted electron mobility (Table 5 and Figure 19b) of electron-only device were 1.70 x 10^{-6} cm^{2}S^{-1}V^{-1}, 1.60 x 10^{-6} cm^{2}S^{-1}V^{-1}, 5.34 x 10^{-6} cm^{2}S^{-1}V^{-1}, 2.30 x 10^{-5} cm^{2}S^{-1}V^{-1} and 2.07 x 10^{-5} cm^{2}S^{-1}V^{-1} for devices made from ETL doped with 0, 1, 2, 3 and 5 wt.% of Sn respectively. Due to the incorporation of the Sn dopant in the ETL, the field-dependent electron mobility increased by one order of magnitude from 10^{-5} cm^{2}S^{-1}V^{-1} to 10^{-4} cm^{2}S^{-1}V^{-1} with the device at an optimum concentration (3 wt.%) exhibited the highest electron mobility. This is a clear indication of an enhanced charge transport process in the device with ETL incorporated with Sn as manifested by reduced R_s and improved FF and V_{oc}. Moreover, the higher electron mobility in 3wt. %-based device reduced the likelihood of exciton recombination,

resulting in a higher FF value, which is consistent with the photovoltaic performance shown in Table 3. The higher zero-field mobility of the absorber layer provides a higher PCE due to a direct relationship between values of overall PCE with zero-field mobility of the OSCs (Hamed et al., 2021). Moreover, the negative value (see Table 5) of γ is the indication of the reduction in mobility at the high applied electric field in the polymer medium (Ike et al., 2022).

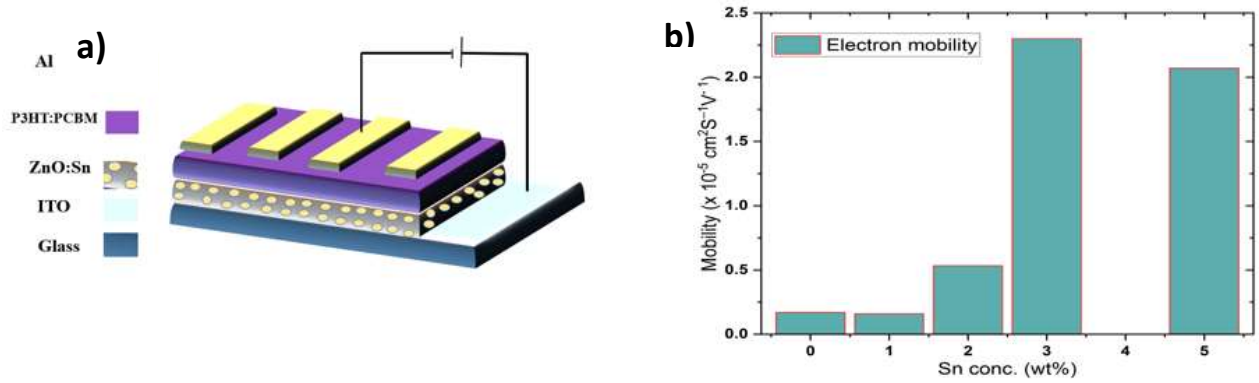

Figure 19. *(a) Schematic device structure of electron-only device, (b) electron mobility using an ITO/ZnO/P3HT: PCBM/Al structure with pristine ZnO and ZnO doped with different concentration of Sn.*

Table 5. The charge transport parameters of the fabricated electron-only device with different concentration of Sn

Sn conc. (wt. %)	μ_e ($cm^2S^{-1}V^{-1}$)	γ (cmV^{-1}) x10^{-4}
0	1.70 x 10^{-6}	-4.55
1	1.60 x 10^{-6}	-6.58
2	5.34 x 10^{-6}	-3.13
3	2.30 x 10^{-5}	-4.40
5	2.07 x 10^{-5}	-4.72

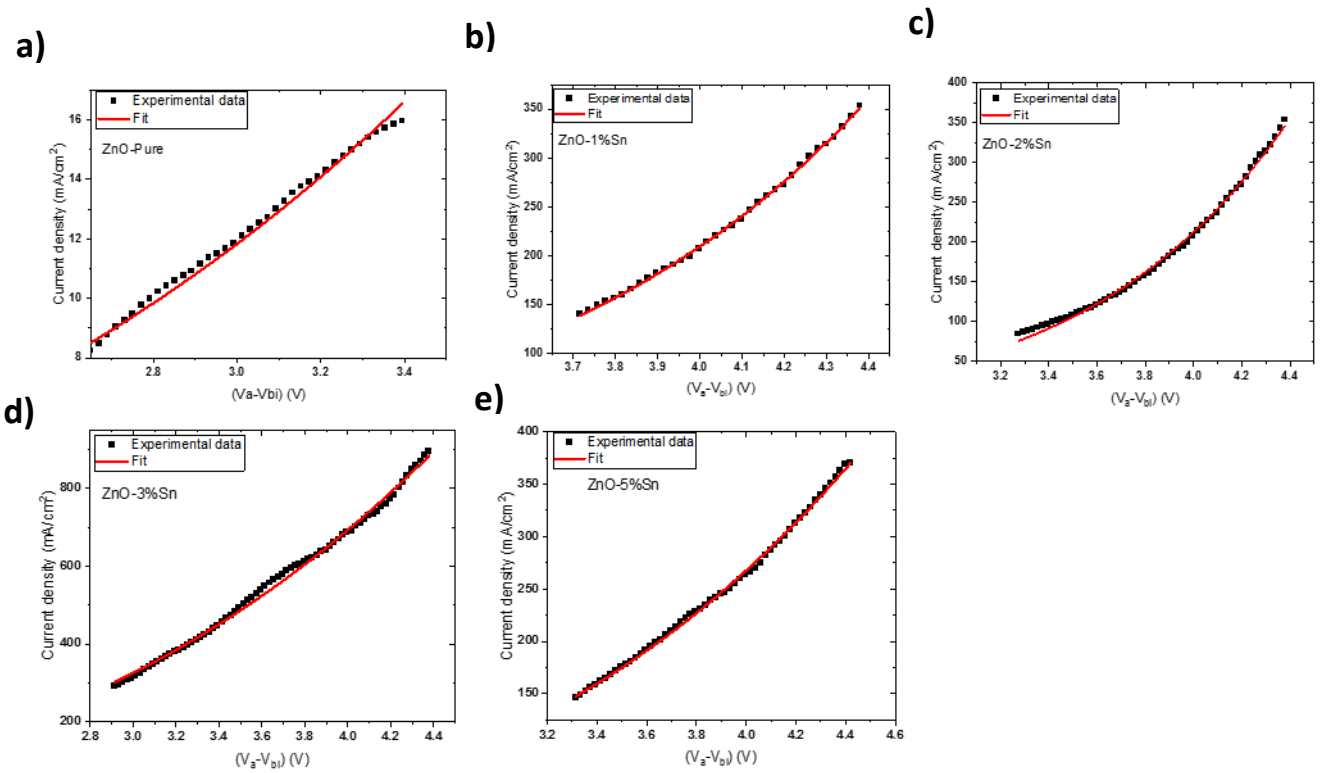

Figure 20*. The space charge limited current of electron-only device fabricated with pristine ZnO and ZnO incorporated with different concentration of Sn. The red line are the fit curves according to Mott-Gurney law to the experimental data points.*

5. CONCLUSION

In conclusion, Pristine and Sn-doped ZnO films as electron transport layers were synthesized using the room temperature sol-gel method. Though systematic characterizations of the synthesized films, we found that the optical and electrical properties of Sn doped ZnO ETL were superior to that of pristine ZnO films in an inverted P3HT-based solar cells. The fabricated solar cells made from ETL doped with Sn showed remarkable improvement in device performances i.e. improved the solar cell parameters such as the open-circuit voltage (V_{oc}), short-circuit current densities (J_{sc}) and fill factor (FF). Subsequently, from the device with 3 wt. % Sn doped, a PCE of about 3.45 % was recorded, which is an improvement of nearly 340 % compared to pure ZnO-based device. The PCE improvement at this doping level was attributed to the combination effect of increased charge mobility in the active layer, effective exciton dissociation at D/A interface, and high light absorption. This device also exhibited a high FF of about 53 %, which could be due to the rougher surface which can increases the contact area at the ETL-active layer interface, low series resistance and bimolecular recombination as confirmed by the higher PL quenching efficiency. The superior value of J_{sc} measured at 5 % concentration of Sn by weight is attributed to its high electrical conductivity which facilitate the charge transport and collection process from the active layer to the electron transport layer and ITO respectively. Therefore, our findings presented herein prove the functionality of Sn doped ZnO as effective ETLs for improving the performance of organic photovoltaics.

6. REFERENCES

Adedeji, M. A., Hamed, M. S., & Mola, G. T. (2020). Light trapping using copper decorated nano-composite in the hole transport layer of organic solar cell. *Solar Energy, 203*, 83-90.

Agnihotri, P., Sahu, S., & Tiwari, S. (2017). *Recent advances & perspectives in electron transport layer of organic solar cells for efficient solar energy harvesting.* Paper presented at the 2017 International Conference on Energy, Communication, Data Analytics and Soft Computing (ICECDS).

Ajili, M., Castagné, M., & Turki, N. K. (2013). Study on the doping effect of Sn-doped ZnO thin films. *Superlattices and Microstructures, 53*, 213-222.

Alstrup, J., Jørgensen, M., Medford, A. J., & Krebs, F. C. (2010). Ultra fast and parsimonious materials screening for polymer solar cells using differentially pumped slot-die coating. *ACS applied materials & interfaces, 2*(10), 2819-2827.

Ameen, S., Akhtar, M. S., Shin, H.-S., & Nazeeruddin, M. K. (2018). Charge-transporting materials for perovskite solar cells. *Advances in Inorganic Chemistry, 72*, 185-246.

Amollo, T. A., Mola, G. T., & Nyamori, V. O. (2020). Improved short-circuit current density in bulk heterojunction solar cells with reduced graphene oxide-germanium dioxide nanocomposite in the photoactive layer. *Materials Chemistry and Physics, 254*, 123448.

Andolsi, Y., Chaabouni, F., & Abaab, M. (2017). Sn doping effects on properties of ZnO thin films deposited by RF magnetron sputtering using a powder target. *Journal of Materials Science: Materials in Electronics, 28*(12), 8347-8358.

Ansari, M. I. H., Qurashi, A., & Nazeeruddin, M. K. (2018). Frontiers, opportunities, and challenges in perovskite solar cells: A critical review. *Journal of Photochemistry and Photobiology C: Photochemistry Reviews, 35*, 1-24. doi: https://doi.org/10.1016/j.jphotochemrev.2017.11.002

Baglio, V., Girolamo, M., Antonucci, V., & Aricò, A. (2011). Influence of TiO2 film thickness on the electrochemical behaviour of dye-sensitized solar cells. *Int. J. Electrochem. Sci, 6*(8), 3375-3384.

Bai, S., Jin, Y., Liang, X., Ye, Z., Wu, Z., Sun, B., . . . Würfel, U. (2015). Ethanedithiol treatment of solution-processed ZnO thin films: controlling the intragap states of electron transporting interlayers for efficient and stable inverted organic photovoltaics. *Advanced Energy Materials, 5*(5), 1401606.

Baranovskii, S., Cordes, H., Hensel, F., & Leising, G. (2000). Charge-carrier transport in disordered organic solids. *Physical Review B, 62*(12), 7934.

Bartesaghi, D., Pérez, I. D. C., Kniepert, J., Roland, S., Turbiez, M., Neher, D., & Koster, L. (2015). Competition between recombination and extraction of free charges determines the fill factor of organic solar cells. *Nature communications, 6*(1), 1-10.

Bedia, F., Bedia, A., Aillerie, M., Maloufi, N., & Benyoucef, B. (2015). Structural, optical and electrical properties of Sn-doped zinc oxide transparent films interesting for organic solar cells (OSCs). *Energy procedia, 74*, 539-546.

Bedia, F. Z., Bedia, A., Maloufi, N., Aillerie, M., Genty, F., & Benyoucef, B. (2014). Effect of tin doping on optical properties of nanostructured ZnO thin films grown by spray pyrolysis technique. *Journal of alloys and compounds, 616*, 312-318.

Bilby, D., Frieberg, B., Kramadhati, S., Green, P., & Kim, J. (2014). Design considerations for electrode buffer layer materials in polymer solar cells. *ACS applied materials & interfaces, 6*(17), 14964-14974.

Blakesley, J. C., Castro, F. A., Kylberg, W., Dibb, G. F., Arantes, C., Valaski, R., . . . Kim, J.-S. (2014). Towards reliable charge-mobility benchmark measurements for organic semiconductors. *Organic Electronics, 15*(6), 1263-1272.

Blakesley, J. C., & Neher, D. (2011). Relationship between energetic disorder and open-circuit voltage in bulk heterojunction organic solar cells. *Physical Review B, 84*(7), 075210.

Blom, P. W., Mihailetchi, V. D., Koster, L. J. A., & Markov, D. E. (2007). Device physics of polymer: fullerene bulk heterojunction solar cells. *Advanced Materials, 19*(12), 1551-1566.

Bob, B., Song, T.-B., Chen, C.-C., Xu, Z., & Yang, Y. (2013). Nanoscale dispersions of gelled Sno2: Material properties and device applications. *Chemistry of Materials, 25*(23), 4725-4730.

Bolognesi, M. (2013). *Organic bulk-heterojunction photovoltaic devices: materials, device architectures and interfacial processes.* Universitat Rovira i Virgili.

Bomila, R., Srinivasan, S., Venkatesan, A., Bharath, B., & Perinbam, K. (2018). Structural, optical and antibacterial activity studies of Ce-doped ZnO nanoparticles prepared by wet-chemical method. *Materials Research Innovations, 22*(7), 379-386.

Braid, J. L. (2016). *Understanding efficiency improvement in organic photovoltaics with molecular modifiers*: Colorado School of Mines.

Bruder, I. (2010). Organic solar cells: Correlation between molecular structure, morphology and device performance.

Carter, S., Angelopoulos, M., Karg, S., Brock, P., & Scott, J. (1997). Polymeric anodes for improved polymer light-emitting diode performance. *Applied Physics Letters, 70*(16), 2067-2069.

Chambon, S., Derue, L., Lahaye, M., Pavageau, B., Hirsch, L., & Wantz, G. (2012). MoO3 thickness, thermal annealing and solvent annealing effects on inverted and direct polymer photovoltaic solar cells. *Materials, 5*(12), 2521-2536.

Chen, H.-C., Lin, S.-W., Jiang, J.-M., Su, Y.-W., & Wei, K.-H. (2015). Solution-processed zinc oxide/polyethylenimine nanocomposites as tunable electron transport layers for highly efficient bulk heterojunction polymer solar cells. *ACS applied materials & interfaces, 7*(11), 6273-6281.

Chen, L. M., Hong, Z., Li, G., & Yang, Y. (2009). Recent progress in polymer solar cells: manipulation of polymer: fullerene morphology and the formation of efficient inverted polymer solar cells. *Advanced Materials, 21*(14-15), 1434-1449.

Chen, Z., Pan, D., Li, Z., Jiao, Z., Wu, M., Shek, C.-H., . . . Lai, J. K. (2014). Recent advances in tin dioxide materials: some developments in thin films, nanowires, and nanorods. *Chemical reviews, 114*(15), 7442-7486.

Cho, J. M., Kwak, S.-W., Aqoma, H., Kim, J. W., Shin, W. S., Moon, S.-J., . . . Jo, J. (2014). Effects of ultraviolet–ozone treatment on organic-stabilized ZnO nanoparticle-based electron transporting layers in inverted polymer solar cells. *Organic Electronics, 15*(9), 1942-1950.

Choi, J., Jo, J. W., de Arquer, F. P. G., Zhao, Y. B., Sun, B., Kim, J., . . . Seifitokaldani, A. (2018). Activated Electron-Transport Layers for Infrared Quantum Dot Optoelectronics. *Advanced Materials, 30*(29), 1801720.

Chou, C.-H., & Chen, F.-C. (2014). Plasmonic nanostructures for light trapping in organic photovoltaic devices. *Nanoscale, 6*(15), 8444-8458.

Cowan, S. R., Roy, A., & Heeger, A. J. (2010). Recombination in polymer-fullerene bulk heterojunction solar cells. *Physical Review B, 82*(24), 245207.

Deibel, C., & Dyakonov, V. (2010). Polymer–fullerene bulk heterojunction solar cells. *Reports on Progress in Physics, 73*(9), 096401.

Dlamini, M. W., Mbuyise, X. G., & Mola, G. T. (2022). ZnO: Ag nano-particles decorated hole transport layer for improved photon harvesting. *Applied Physics A, 128*(2), 1-10.

Eita, M., Labban, A. E., Cruciani, F., Usman, A., Beaujuge, P. M., & Mohammed, O. F. (2015). Ambient Layer-by-Layer Zno Assembly for Highly Efficient Polymer Bulk Heterojunction Solar Cells. *Advanced Functional Materials, 25*(10), 1558-1564.

ETHIOPIA, O. Ethiopia's Climate-Resilient Green Economy Strategy.

Facchetti, A. (2013). Polymer donor–polymer acceptor (all-polymer) solar cells. *Materials today, 16*(4), 123-132.

Fung, D. D., & Choy, W. C. (2013). Experimental studies of plasmonic nanoparticle effects on organic solar cells *Organic Solar Cells* (pp. 211-242): Springer.

Ganesh, V., Yahia, I., AlFaify, S., & Shkir, M. (2017). Sn-doped ZnO nanocrystalline thin films with enhanced linear and nonlinear optical properties for optoelectronic applications. *Journal of Physics and Chemistry of Solids, 100*, 115-125.

Gehrig, D. (2015). *Unraveling efficiency-limiting processes in organic solar cells by ultrafast spectroscopy-impact of chemical structure and morphology on photophysics and efficency.* Johannes Gutenberg-Universität Mainz.

Girotto, C., Rand, B. P., Steudel, S., Genoe, J., & Heremans, P. (2009). Nanoparticle-based, spray-coated silver top contacts for efficient polymer solar cells. *Organic Electronics, 10*(4), 735-740.

Guo, L., Yang, S., Yang, C., Yu, P., Wang, J., Ge, W., & Wong, G. K. (2000). Highly monodisperse polymer-capped ZnO nanoparticles: Preparation and optical properties. *Applied Physics Letters, 76*(20), 2901-2903.

Hadipour, A., Müller, R., & Heremans, P. (2013). Room temperature solution-processed electron transport layer for organic solar cells. *Organic Electronics, 14*(10), 2379-2386.

Hamed, M. S., Ike, J. N., & Mola, G. T. (2021). Plasmonic nano-particles mediated energy harvesting in thin-film organic solar cells. *Journal of Physics D: Applied Physics, 55*(1), 015102.

Han, B., Gopalan, S.-A., Lee, K.-D., Kang, B.-H., Lee, S.-W., Lee, J.-S., . . . Kang, S.-W. (2014). Preheated solvent exposure on P3HT: PCBM thin film: A facile strategy to enhance performance in bulk heterojunction photovoltaic cells. *Current Applied Physics, 14*(11), 1443-1450.

Hau, S. K., Cheng, Y.-J., Yip, H.-L., Zhang, Y., Ma, H., & Jen, A. K.-Y. (2010). Effect of chemical modification of fullerene-based self-assembled monolayers on the performance of inverted polymer solar cells. *ACS applied materials & interfaces, 2*(7), 1892-1902.

He, Z., Zhong, C., Su, S., Xu, M., Wu, H., & Cao, Y. (2012). Enhanced power-conversion efficiency in polymer solar cells using an inverted device structure. *Nature Photonics, 6*(9), 591-595.

Homnan, S., Malison, P., Amratisha, K., Kanjanaboos, P., Wongratanaphisan, D., Sagawa, T., & Ruankham, P. (2021). Low-temperature processable Sn-doped ZnO films as electron transporting layers for perovskite solar cells. *Journal of Materials Science: Materials in Electronics, 32*(23), 27279-27289.

Hu, T., Chen, L., Yuan, K., & Chen, Y. (2015). Amphiphilic fullerene/ZnO hybrids as cathode buffer layers to improve charge selectivity of inverted polymer solar cells. *Nanoscale, 7*(20), 9194-9203.

Hu, Z., Zhang, J., Liu, Y., Hao, Z., Zhang, X., & Zhao, Y. (2011). Influence of ZnO interlayer on the performance of inverted organic photovoltaic device. *Solar Energy Materials and Solar Cells, 95*(8), 2126-2130.

Huang, J.-S., Chou, C.-Y., & Lin, C.-F. (2010). Enhancing performance of organic–inorganic hybrid solar cells using a fullerene interlayer from all-solution processing. *Solar Energy Materials and Solar Cells, 94*(2), 182-186.

Humayun, Q., Kashif, M., & Hashim, U. (2013). Structural, optical, electrical, and photoresponse properties of postannealed Sn-doped ZnO nanorods. *Journal of Nanomaterials, 2013*.

Ibrahem, M. A., Wei, H.-Y., Tsai, M.-H., Ho, K.-C., Shyue, J.-J., & Chu, C. W. (2013). Solution-processed zinc oxide nanoparticles as interlayer materials for inverted organic solar cells. *Solar Energy Materials and Solar Cells, 108*, 156-163.

Ike, J. N., Hamed, M. S., & Mola, G. T. (2022). Effective energy harvesting in thin film organic solar cells using Ni: Zn as bimetallic nanoparticles. *Journal of Physics and Chemistry of Solids, 161*, 110405.

Ikram, M., Murray, R., Imran, M., Ali, S., & Shah, S. I. (2016). Enhanced performance of P3HT/(PCBM: ZnO: TiO2) blend based hybrid organic solar cells. *Materials Research Bulletin, 75*, 35-40.

Ilican, S., Caglar, M., & Caglar, Y. (2010). Sn doping effects on the electro-optical properties of sol gel derived transparent ZnO films. *Applied Surface Science, 256*(23), 7204-7210.

Ionescu-Zanetti, C., Mechler, A., Carter, S. A., & Lal, R. (2004). Semiconductive polymer blends: Correlating structure with transport properties at the nanoscale. *Advanced Materials, 16*(5), 385-389.

Jagadamma, L. K., Al-Senani, M., El-Labban, A., Gereige, I., Ngongang Ndjawa, G. O., Faria, J. C., . . . Anjum, D. H. (2015). Polymer solar cells with efficiency> 10% enabled via a facile solution-processed Al-doped ZnO electron transporting layer. *Advanced Energy Materials, 5*(12), 1500204.

Jaumot, J., Gargallo, R., De Juan, A., & Tauler, R. (2005). A graphical user-friendly interface for MCR-ALS: a new tool for multivariate curve resolution in MATLAB. *Chemometrics and intelligent laboratory systems, 76*(1), 101-110.

Jørgensen, M., Norrman, K., Gevorgyan, S. A., Tromholt, T., Andreasen, B., & Krebs, F. C. (2012). Stability of polymer solar cells. *Advanced Materials, 24*(5), 580-612.

Kawano, K., Pacios, R., Poplavskyy, D., Nelson, J., Bradley, D. D., & Durrant, J. R. (2006). Degradation of organic solar cells due to air exposure. *Solar Energy Materials and Solar Cells, 90*(20), 3520-3530.

Keivanidis, P. E., Howard, I. A., & Friend, R. H. (2008). Intermolecular interactions of perylene diimides in photovoltaic blends of fluorene copolymers: disorder effects on photophysical properties, film morphology and device efficiency. *Advanced Functional Materials, 18*(20), 3189-3202.

Kemerink, M., Timpanaro, S., De Kok, M., Meulenkamp, E., & Touwslager, F. (2004). Three-dimensional inhomogeneities in PEDOT: PSS films. *The Journal of Physical Chemistry B, 108*(49), 18820-18825.

Kemerink, M., Van Duren, J., Jonkheijm, P., Pasveer, W., Koenraad, P., Janssen, R., . . . Wolter, J. (2003). Relating substitution to single-chain conformation and aggregation in poly (p-phenylene vinylene) films. *Nano letters, 3*(9), 1191-1196.

Kim, Y. J., Ahn, S., Wang, D. H., & Park, C. E. (2015). A mechanistic understanding of a binary additive system to synergistically boost efficiency in all-polymer solar cells. *Scientific reports, 5*(1), 1-13.

Krebs, F. C. (2009). All solution roll-to-roll processed polymer solar cells free from indium-tin-oxide and vacuum coating steps. *Organic Electronics, 10*(5), 761-768.

Krebs, F. C., Gevorgyan, S. A., & Alstrup, J. (2009). A roll-to-roll process to flexible polymer solar cells: model studies, manufacture and operational stability studies. *Journal of Materials Chemistry, 19*(30), 5442-5451.

Krebs, F. C., Tromholt, T., & Jørgensen, M. (2010). Upscaling of polymer solar cell fabrication using full roll-to-roll processing. *Nanoscale, 2*(6), 873-886.

Kumar, A. S., Huang, N., & Nagaraja, H. (2014). Influence of Sn doping on photoluminescence and photoelectrochemical properties of ZnO nanorod arrays. *Electronic Materials Letters, 10*(4), 753-758.

Kumar, M., Bhatt, V., Abhyankar, A., Kim, J., Kumar, A., & Yun, J.-H. (2018). Modulation of structural properties of Sn doped ZnO for UV photoconductors. *Sensors and Actuators A: Physical, 270*, 118-126.

Kyaw, A. K. K., Sun, X., Tan, S. T., Divayana, Y., & Demir, H. V. (2010). Improved inverted organic solar cells with a sol–gel derived indium-doped zinc oxide buffer layer. *IEEE Journal of Selected Topics in Quantum Electronics, 16*(6), 1700-1706.

Lattante, S. (2014). Electron and hole transport layers: their use in inverted bulk heterojunction polymer solar cells. *Electronics, 3*(1), 132-164.

Lattante, S., Perulli, A., & Anni, M. (2011). Study of the series resistance evolution in organic solar cells by use of the Lambert W function. *Synthetic Metals, 161*(11-12), 949-952.

Law, M., Greene, L., & Johnson, J. (2005). R. saykally, PD Yang. *Nat. Mater, 4*, 455.

Lee, J.-Y., Kim, S.-H., Song, I.-S., & Moon, D.-K. (2011). Efficient donor–acceptor type polymer semiconductors with well-balanced energy levels and enhanced open circuit voltage properties for use in organic photovoltaics. *Journal of Materials Chemistry, 21*(41), 16480-16487.

Lee, J. M., Lim, J., Lee, N., Park, H. I., Lee, K. E., Jeon, T., . . . Kim, S. O. (2015). Synergistic concurrent enhancement of charge generation, dissociation, and transport in organic solar cells with plasmonic metal–carbon nanotube hybrids. *Advanced Materials, 27*(9), 1519-1525.

Lee, S.-H., Kim, J.-H., Shim, T.-H., & Park, J.-G. (2009). Effect of interface thickness on power conversion efficiency of polymer photovoltaic cells. *Electronic Materials Letters, 5*(1), 47-50.

Lenes, M., Morana, M., Brabec, C. J., & Blom, P. W. (2009). Recombination-limited photocurrents in low bandgap polymer/fullerene solar cells. *Advanced Functional Materials, 19*(7), 1106-1111.

Li, J., Ren, M., Qing, J., Wang, Y., Liang, Z., Wang, N., . . . Xia, Y. (2019). Solution-processible Cd-doped ZnO nanoparticles as an electron transport layer to achieve high performance polymer solar cells through improve conductivity and light transmittance. *Molecular Crystals and Liquid Crystals, 692*(1), 74-82.

Liang, Z., Zhang, Q., Jiang, L., & Cao, G. (2015). ZnO cathode buffer layers for inverted polymer solar cells. *Energy & Environmental Science, 8*(12), 3442-3476.

Liang, Z., Zhang, Q., Wiranwetchayan, O., Xi, J., Yang, Z., Park, K., . . . Cao, G. (2012). Effects of the morphology of a ZnO buffer layer on the photovoltaic performance of inverted polymer solar cells. *Advanced Functional Materials, 22*(10), 2194-2201.

Liao, S.-H., Jhuo, H.-J., Yeh, P.-N., Cheng, Y.-S., Li, Y.-L., Lee, Y.-H., . . . Chen, S.-A. (2014). Single junction inverted polymer solar cell reaching power conversion efficiency 10.31% by employing dual-doped zinc oxide nano-film as cathode interlayer. *Scientific reports, 4*(1), 1-7.

Liao, S. H., Jhuo, H. J., Cheng, Y. S., & Chen, S. A. (2013). Fullerene derivative-doped zinc oxide nanofilm as the cathode of inverted polymer solar cells with low-bandgap polymer (PTB7-Th) for high performance. *Advanced Materials, 25*(34), 4766-4771.

Lilliedal, M. R., Medford, A. J., Madsen, M. V., Norrman, K., & Krebs, F. C. (2010). The effect of post-processing treatments on inflection points in current–voltage curves of roll-to-roll processed polymer photovoltaics. *Solar Energy Materials and Solar Cells, 94*(12), 2018-2031.

Lin, Y., Hsu, C., Hung, S.-K., Chang, C., & Wen, D. (2012). The structural and optoelectronic properties of Ti-doped ZnO thin films prepared by introducing a Cr buffer layer and post-annealing. *Applied Surface Science, 258*(24), 9891-9895.

Lin, Y., Nugraha, M. I., Firdaus, Y., Scaccabarozzi, A. D., Aniés, F., Emwas, A.-H., . . . Wahyudi, W. (2020). A simple n-dopant derived from diquat boosts the efficiency of organic solar cells to 18.3%. *ACS Energy Letters, 5*(12), 3663-3671.

Litzov, I., & Brabec, C. J. (2013). Development of efficient and stable inverted bulk heterojunction (BHJ) solar cells using different metal oxide interfaces. *Materials, 6*(12), 5796-5820.

Lloyd, M. T., Olson, D. C., Lu, P., Fang, E., Moore, D. L., White, M. S., . . . Hsu, J. W. (2009). Impact of contact evolution on the shelf life of organic solar cells. *Journal of Materials Chemistry, 19*(41), 7638-7642.

Ma, W., Tumbleston, J. R., Ye, L., Wang, C., Hou, J., & Ade, H. (2014). Quantification of nano- and mesoscale phase separation and relation to donor and acceptor quantum efficiency, Jsc, and FF in polymer: fullerene solar cells. *Advanced Materials, 26*(25), 4234-4241.

Ma, Z., Tang, Z., Wang, E., Andersson, M. R., Inganäs, O., & Zhang, F. (2012). Influences of surface roughness of ZnO electron transport layer on the photovoltaic performance of organic inverted solar cells. *The Journal of Physical Chemistry C, 116*(46), 24462-24468.

Mahmood, K., Sarwar, S., & Mehran, M. T. (2017). Current status of electron transport layers in perovskite solar cells: materials and properties. *RSC advances, 7*(28), 17044-17062.

Malison, P., Bhoomanee, C., Choopun, S., Wongratanaphisan, D., Sagawa, T., & Ruankham, P. (2019). *Effects of Sn Incorporation in ZnO Thin Films on Properties of Perovskite Solar Cells.* Paper presented at the IOP Conference Series: Materials Science and Engineering.

Mayer, A. C., Scully, S. R., Hardin, B. E., Rowell, M. W., & McGehee, M. D. (2007). Polymer-based solar cells. *Materials today, 10*(11), 28-33.

Meyer, J., Hamwi, S., Bülow, T., Johannes, H.-H., Riedl, T., & Kowalsky, W. (2007). Highly efficient simplified organic light emitting diodes. *Applied Physics Letters, 91*(11), 113506.

Mihailetchi, V. D. (2005). Device physics of organic bulk heterojunction solar cells. *Rijksuniversiteit Groningen, Niederlande, Doktorarbeit*.

Mihailetchi, V. D., & Xie, H. (2006). B. de [thin space (1/6-em)] Boer, LJA Koster and PWM Blom. *Adv. Funct. Mater, 16*, 699-708.

Mott, N. (1940). RW Gurney Electronic Processes in Ionic Crystals.

Nair, M. G., Nirmala, M., Rekha, K., & Anukaliani, A. (2011). Structural, optical, photo catalytic and antibacterial activity of ZnO and Co doped ZnO nanoparticles. *Materials Letters, 65*(12), 1797-1800.

Nickel, F., Sprau, C., Klein, M. F., Kapetana, P., Christ, N., Liu, X., . . . Colsmann, A. (2012). Spatial mapping of photocurrents in organic solar cells comprising wedge-shaped absorber layers for an efficient material screening. *Solar Energy Materials and Solar Cells, 104*, 18-22.

Nicolai, H., & Kuik, M. (2012). G. a. H. Wetzelaer, B. de Boer, C. Campbell, C. Risko, JL Brédas and PWM Blom. *Nat. Mater, 11*, 882-887.

Oh, H., Krantz, J., Litzov, I., Stubhan, T., Pinna, L., & Brabec, C. J. (2011). Comparison of various sol–gel derived metal oxide layers for inverted organic solar cells. *Solar Energy Materials and Solar Cells, 95*(8), 2194-2199.

Ohyama, M., Kouzuka, H., & Yoko, T. (1997). Sol-gel preparation of ZnO films with extremely preferred orientation along (002) plane from zinc acetate solution. *Thin Solid Films, 306*(1), 78-85.

Ohyama, M., Kozuka, H., & Yoko, T. (1998). Sol-gel preparation of transparent and conductive aluminum-doped zinc oxide films with highly preferential crystal orientation. *Journal of the American Ceramic Society, 81*(6), 1622-1632.

Park, H.-Y., Lim, D., Kim, K.-D., & Jang, S.-Y. (2013). Performance optimization of low-temperature-annealed solution-processable ZnO buffer layers for inverted polymer solar cells. *Journal of Materials Chemistry A, 1*(21), 6327-6334.

Peng, H., Xu, W., Zhou, F., Zhang, J., & Li, C. (2015). Enhanced efficiency of inverted polymer solar cells using surface modified Cs-doped ZnO as electron transporting layer. *Synthetic Metals, 205*, 164-168.

Peng, R., Yang, F., Ouyang, X., Liu, Y., Kim, Y.-S., & Ge, Z. (2013). Enhanced photovoltaic performance of inverted polymer solar cells by tuning the structures of titanium dioxide. *Thin Solid Films, 545*, 424-428.

Peumans, P., Yakimov, A., & Forrest, S. R. (2003). Small molecular weight organic thin-film photodetectors and solar cells. *Journal of Applied Physics, 93*(7), 3693-3723.

Pitchaiya, S., Natarajan, M., Santhanam, A., Asokan, V., Yuvapragasam, A., Ramakrishnan, V. M., . . . Velauthapillai, D. (2020). A review on the classification of organic/inorganic/carbonaceous hole transporting materials for perovskite solar cell application. *Arabian Journal of Chemistry, 13*(1), 2526-2557.

Pivrikas, A., Sariciftci, N. S., Juška, G., & Österbacka, R. (2007). A review of charge transport and recombination in polymer/fullerene organic solar cells. *Progress in Photovoltaics: Research and Applications, 15*(8), 677-696.

Po, R., Carbonera, C., Bernardi, A., & Camaioni, N. (2011). The role of buffer layers in polymer solar cells. *Energy & Environmental Science, 4*(2), 285-310.

Qiu, Z., Yuan, S., Gong, H., Zhang, H., Qiu, X., Luo, T., & Cao, B. (2017). The influence of physical properties of ZnO films on the efficiency of planar ZnO/perovskite/P3HT solar cell. *Journal of the American Ceramic Society, 100*(1), 176-184.

Rafique, S., Abdullah, S. M., Sulaiman, K., & Iwamoto, M. (2018). Fundamentals of bulk heterojunction organic solar cells: An overview of stability/degradation issues and strategies for improvement. *Renewable and Sustainable Energy Reviews, 84*, 43-53.

Ren, H., Sun, S., Cui, J., & Li, X. (2018). Synthesis, functional modifications, and diversified applications of molybdenum oxides micro-/nanocrystals: A review. *Crystal Growth & Design, 18*(10), 6326-6369.

Rherari, A., Addou, M., Bougrine, A., El Jouad, M., & Haris, M. Linear and Non Linear Optical Parameters of TZO Thin Films Prepared by Spray Pyrolysis.

Roy, P., Kumar Sinha, N., Tiwari, S., & Khare, A. (2020). A review on perovskite solar cells: Evolution of architecture, fabrication techniques, commercialization issues and status. *Solar Energy, 198*, 665-688. doi: https://doi.org/10.1016/j.solener.2020.01.080

Roy, P., Sinha, N. K., Tiwari, S., & Khare, A. (2020). A review on perovskite solar cells: Evolution of architecture, fabrication techniques, commercialization issues and status. *Solar Energy, 198*, 665-688.

Sakohara, S., Ishida, M., & Anderson, M. A. (1998). Visible luminescence and surface properties of nanosized ZnO colloids prepared by hydrolyzing zinc acetate. *The Journal of Physical Chemistry B, 102*(50), 10169-10175.

Samavati, A., Samavati, Z., Ismail, A., Othman, M., Rahman, M. A., Zulhairun, A., & Amiri, I. (2017). Structural, optical and electrical evolution of Al and Ga co-doped ZnO/SiO 2/glass thin film: role of laser power density. *RSC advances, 7*(57), 35858-35868.

Sasajima, I., Uesaka, S., Kuwabara, T., Yamaguchi, T., & Takahashi, K. (2011). Flexible inverted polymer solar cells containing an amorphous titanium oxide electron collection electrode. *Organic Electronics, 12*(1), 113-118.

Scharber, M. C., & Sariciftci, N. S. (2013). Efficiency of bulk-heterojunction organic solar cells. *Progress in polymer science, 38*(12), 1929-1940.

Schumann, S., Da Campo, R., Illy, B., Cruickshank, A., McLachlan, M., Ryan, M., . . . Jones, T. (2011). Inverted organic photovoltaic devices with high efficiency and stability based on metal oxide charge extraction layers. *Journal of Materials Chemistry, 21*(7), 2381-2386.

Servaites, J. D., Ratner, M. A., & Marks, T. J. (2011). Organic solar cells: A new look at traditional models. *Energy & Environmental Science, 4*(11), 4410-4422.

Sharenko, A., Proctor, C. M., van der Poll, T. S., Henson, Z. B., Nguyen, T. Q., & Bazan, G. C. (2013). A High-Performing Solution-Processed Small Molecule: Perylene Diimide Bulk Heterojunction Solar Cell. *Advanced Materials, 25*(32), 4403-4406.

Shockley, W., & Queisser, H. J. (1961). Detailed balance limit of efficiency of p-n junction solar cells. *Journal of Applied Physics, 32*(3), 510-519.

Singh, P., Kumar, R., & Singh, R. K. (2020). Fabrication of Co-and Ce-doped ZnO nanoparticles: a structural, morphological and optical properties investigation. *Applied Nanoscience, 10*(4), 1231-1241.

Singh, P., Singh, R. K., & Kumar, R. (2021). Journey of ZnO quantum dots from undoped to rare-earth and transition metal-doped and their applications. *RSC advances, 11*(4), 2512-2545.

Small, C. E., Chen, S., Subbiah, J., Amb, C. M., Tsang, S.-W., Lai, T.-H., . . . So, F. (2012). High-efficiency inverted dithienogermole–thienopyrrolodione-based polymer solar cells. *Nature Photonics, 6*(2), 115-120.

Søndergaard, R. R., Hösel, M., & Krebs, F. C. (2013). Roll-to-Roll fabrication of large area functional organic materials. *Journal of Polymer Science Part B: Polymer Physics, 51*(1), 16-34.

Steim, R., Kogler, F. R., & Brabec, C. J. (2010). Interface materials for organic solar cells. *Journal of Materials Chemistry, 20*(13), 2499-2512.

Steyrleuthner, R., Schubert, M., Jaiser, F., Blakesley, J. C., Chen, Z., Facchetti, A., & Neher, D. (2010). Bulk Electron Transport and Charge Injection in a High Mobility n-Type Semiconducting Polymer. *Advanced Materials, 22*(25), 2799-2803.

Stubhan, T., Oh, H., Pinna, L., Krantz, J., Litzov, I., & Brabec, C. J. (2011). Inverted organic solar cells using a solution processed aluminum-doped zinc oxide buffer layer. *Organic Electronics, 12*(9), 1539-1543.

Stubhan, T., Salinas, M., Ebel, A., Krebs, F. C., Hirsch, A., Halik, M., & Brabec, C. J. (2012). Increasing the Fill Factor of Inverted P3HT: PCBM Solar Cells Through Surface Modification of Al-Doped ZnO via Phosphonic Acid-Anchored C60 SAMs. *Advanced Energy Materials, 2*(5), 532-535.

Sun, J., Zhu, Y., Xu, X., Lan, L., Zhang, L., Cai, P., . . . Cao, Y. (2012). High efficiency and high V oc inverted polymer solar cells based on a low-lying HOMO polycarbazole donor and a hydrophilic polycarbazole interlayer on ITO cathode. *The Journal of Physical Chemistry C, 116*(27), 14188-14198.

Sun, S.-S., & Dalton, L. R. (2008). *Introduction to organic electronic and optoelectronic materials and devices*: CRC press.

Sun, Y., Seo, J. H., Takacs, C. J., Seifter, J., & Heeger, A. J. (2011). Inverted polymer solar cells integrated with a low-temperature-annealed sol-gel-derived ZnO film as an electron transport layer. *Advanced Materials, 23*(14), 1679-1683.

Sun, Y., Welch, G. C., Leong, W. L., Takacs, C. J., Bazan, G. C., & Heeger, A. J. (2012). Solution-processed small-molecule solar cells with 6.7% efficiency. *Nature materials, 11*(1), 44-48.

Sutton, R. J. (2018). *Towards stable perovskite materials for photovoltaics.* University of Oxford.

Tao, C., Ruan, S., Zhang, X., Xie, G., Shen, L., Kong, X., . . . Chen, W. (2008). Performance improvement of inverted polymer solar cells with different top electrodes by introducing a MoO 3 buffer layer. *Applied Physics Letters, 93*(19), 411.

Tao, H., Ma, Z., Yang, G., Wang, H., Long, H., Zhao, H., . . . Fang, G. (2018). Room-temperature processed tin oxide thin film as effective hole blocking layer for planar perovskite solar cells. *Applied Surface Science, 434*, 1336-1343.

Tegegne, N. (2018). *Photophysics and photovoltaic application of direct heteroarylation derived isoindigo based copolymers.* Stellenbosch: Stellenbosch University.

Thaver, Y., Oseni, S. O., & Mola, G. T. (2021). Silver doped nickel oxide nanocomposite and photon harvesting enhancement in bulkheterojunction organic solar cell. *Solar Energy, 214*, 11-18.

Tsai, S., Ho, S., Jhuo, H., Ho, C., Chen, S., & He, J.-H. (2013). Toward high efficiency of inverted organic solar cells: Concurrent improvement in optical and electrical properties of electron transport layers. *Applied Physics Letters, 102*(25), 253111.

Tu, Q., Cai, D., Wang, L., Wei, J., Shang, Q., Chen, S.-C., . . . Zheng, Q. (2016). Side-chain engineering of diindenocarbazole-based large bandgap copolymers toward high performance polymer solar cells. *Journal of Materials Chemistry C, 4*(25), 6160-6168.

Umar, A., & Hahn, Y. (2006). ZnO nanosheet networks and hexagonal nanodiscs grown on silicon substrate: growth mechanism and structural and optical properties. *Nanotechnology, 17*(9), 2174.

US, E. (2017). Energy Information Administration international energy outlook.

Venkataraj, S., Hishita, S., Adachi, Y., Sakaguchi, I., Matsumoto, K., Saito, N., . . . Ohashi, N. (2009). Structure and electric properties in tin-doped zinc oxide films synthesized by pulsed laser deposition. *Journal of the Electrochemical Society, 156*(6), H424.

Venkatesh, N., Aravindan, S., Ramki, K., Murugadoss, G., Thangamuthu, R., & Sakthivel, P. (2021). Sunlight-driven enhanced photocatalytic activity of bandgap narrowing Sn-doped ZnO nanoparticles. *Environmental Science and Pollution Research, 28*(13), 16792-16803.

Wan, X., Long, G., Huang, L., & Chen, Y. (2011). Graphene–a promising material for organic photovoltaic cells. *Advanced Materials, 23*(45), 5342-5358.

Wang, F., Qiao, X., Xiong, T., & Ma, D. (2008). The role of molybdenum oxide as anode interfacial modification in the improvement of efficiency and stability in organic light-emitting diodes. *Organic Electronics, 9*(6), 985-993.

Wang, J., Lee, Y.-J., Chadha, A. S., Yi, J., Jespersen, M. L., Kelley, J. J., . . . Vaia, R. A. (2013). Effect of plasmonic Au nanoparticles on inverted organic solar cell performance. *The Journal of Physical Chemistry C, 117*(1), 85-91.

Wang, K., Yi, C., Liu, C., Hu, X., Chuang, S., & Gong, X. (2015). Effects of magnetic nanoparticles and external magnetostatic field on the bulk heterojunction polymer solar cells. *Scientific reports, 5*(1), 1-9.

Wang, M., Ren, F., Zhou, J., Cai, G., Cai, L., Hu, Y., . . . Guo, L. (2015). N Doping to ZnO Nanorods for Photoelectrochemical Water Splitting under Visible Light: Engineered Impurity Distribution and Terraced Band Structure. *Scientific reports, 5*, 12925. doi: 10.1038/srep12925

Wang, Z., Helander, M., Greiner, M., Qiu, J., & Lu, Z. (2009). Analysis of charge-injection characteristics at electrode-organic interfaces: Case study of transition-metal oxides. *Physical Review B, 80*(23), 235325.

Wang, Z., Liu, X., Jiang, H., Zhou, X., Zhang, L., Pan, F., . . . Ding, L. (2019). Organic Solar Cells Based on High Hole Mobility Conjugated Polymer and Nonfullerene Acceptor with Comparable Bandgaps and Suitable Energy Level Offsets Showing Significant Suppression of Jsc–Voc Trade-Off. *Solar Rrl, 3*(7), 1900079.

Wei, J., Yin, Z., Chen, S.-C., & Zheng, Q. (2017). Low-temperature solution-processed zinc tin oxide film as a cathode interlayer for organic solar cells. *ACS applied materials & interfaces, 9*(7), 6186-6193.

Wetzelaer, G., Najafi, A., Kist, R., Kuik, M., & Blom, P. W. (2013). Efficient electron injection from solution-processed cesium stearate interlayers in organic light-emitting diodes. *Applied Physics Letters, 102*(5), 22.

White, M.-S., Olson, D., Shaheen, S., Kopidakis, N., & Ginley, D. S. (2006). Inverted bulk-heterojunction organic photovoltaic device using a solution-derived ZnO underlayer. *Applied Physics Letters, 89*(14), 143517.

Wöhrle, D., & Meissner, D. (1991). Organic solar cells. *Advanced Materials, 3*(3), 129-138.

Woo, S., Hyun Kim, W., Kim, H., Yi, Y., Lyu, H. K., & Kim, Y. (2014). 8.9% single-stack inverted polymer solar cells with electron-rich polymer nanolayer-modified inorganic electron-collecting buffer layers. *Advanced Energy Materials, 4*(7), 1301692.

Wu, Q., Chen, X., Zhang, P., Han, Y., Chen, X., Yan, Y., & Li, S. (2008). Amino acid-assisted synthesis of ZnO hierarchical architectures and their novel photocatalytic activities. *Crystal Growth and Design, 8*(8), 3010-3018.

Wu, Q., Wang, W., Wang, T., Sun, R., Guo, J., Wu, Y., . . . Min, J. (2020). High-performance all-polymer solar cells with only 0.47 eV energy loss. *Science China Chemistry, 63*(10), 1449-1460.

Xin, H., Subramaniyan, S., Kwon, T.-W., Shoaee, S., Durrant, J. R., & Jenekhe, S. A. (2012). Enhanced open circuit voltage and efficiency of donor–acceptor copolymer solar cells by using indene-C60 bisadduct. *Chemistry of Materials, 24*(11), 1995-2001.

Xu, H., Yuan, F., Zhou, D., Liao, X., Chen, L., & Chen, Y. (2020). Hole transport layers for organic solar cells: Recent progress and prospects. *Journal of Materials Chemistry A, 8*(23), 11478-11492.

Yang, T., Cai, W., Qin, D., Wang, E., Lan, L., Gong, X., . . . Cao, Y. (2010). Solution-processed zinc oxide thin film as a buffer layer for polymer solar cells with an inverted device structure. *The Journal of Physical Chemistry C, 114*(14), 6849-6853.

Yang, T., Wang, M., Duan, C., Hu, X., Huang, L., Peng, J., . . . Gong, X. (2012). Inverted polymer solar cells with 8.4% efficiency by conjugated polyelectrolyte. *Energy & Environmental Science, 5*(8), 8208-8214.

Yang, Z., Zhang, T., Li, J., Xue, W., Han, C., Cheng, Y., . . . Chen, S. (2017). Multiple electron transporting layers and their excellent properties based on organic solar cell. *Scientific reports, 7*(1), 1-9.

Ye, J., Gu, S., Qin, F., Zhu, S., Liu, S., Zhou, X., . . . Shi, Y. (2005). Correlation between green luminescence and morphology evolution of ZnO films. *Applied Physics A, 81*(4), 759-762.

Yin, Z., Zheng, Q., Chen, S.-C., & Cai, D. (2013). Interface control of semiconducting metal oxide layers for efficient and stable inverted polymer solar cells with open-circuit voltages over 1.0 volt. *ACS applied materials & interfaces, 5*(18), 9015-9025.

Yin, Z., Zheng, Q., Chen, S. C., Cai, D., Zhou, L., & Zhang, J. (2014). Bandgap Tunable Zn1-xMgxO Thin Films as Highly Transparent Cathode Buffer Layers for High-Performance Inverted Polymer Solar Cells. *Advanced Energy Materials, 4*(7), 1301404.

Yip, H.-L., & Jen, A. K.-Y. (2012). Recent advances in solution-processed interfacial materials for efficient and stable polymer solar cells. *Energy & Environmental Science, 5*(3), 5994-6011.

You, J., Chen, C. C., Hong, Z., Yoshimura, K., Ohya, K., Xu, R., . . . Yang, Y. (2013). 10.2% power conversion efficiency polymer tandem solar cells consisting of two identical sub-cells. *Advanced Materials, 25*(29), 3973-3978.

You, J., Dou, L., Yoshimura, K., Kato, T., Ohya, K., Moriarty, T., . . . Li, G. (2013). A polymer tandem solar cell with 10.6% power conversion efficiency. *Nature communications, 4*(1), 1-10.

Yousefi, R., Jamali-Sheini, F., Zak, A. K., & Mahmoudian, M. (2012). Effect of indium concentration on morphology and optical properties of In-doped ZnO nanostructures. *Ceramics International, 38*(8), 6295-6301.

Yu, S., Yang, W., Li, L., & Zhang, W. (2016). Improved chemical stability of ITO transparent anodes with a SnO2 buffer layer for organic solar cells. *Solar Energy Materials and Solar Cells, 144*, 652-656.

Yu, X., Yu, X., Hu, Z., Zhang, J., Zhao, G., & Zhao, Y. (2013). Effect of sol–gel derived ZnO annealing rate on light-trapping in inverted polymer solar cells. *Materials Letters, 108*, 50-53.

Yung, K. C., Liem, H., & Choy, H. (2009). Enhanced redshift of the optical band gap in Sn-doped ZnO free standing films using the sol–gel method. *Journal of Physics D: Applied Physics, 42*(18), 185002.

Zhou, Y., Eck, M., & Krüger, M. (2010). Bulk-heterojunction hybrid solar cells based on colloidal nanocrystals and conjugated polymers. *Energy & Environmental Science, 3*(12), 1851-1864.